

Singularities, geodesics and Green functions in the BTZ black hole

Chen Yang

*Centre for Particle Theory
Department of Mathematical Sciences
University of Durham
Science Laboratories, South Rd,
Durham, DH1 3LE, UK
email: chen.yang2@durham.ac.uk*

December 2, 2024

Abstract

In the context of studying black hole singularities by the AdS/CFT correspondence, we study the BTZ black hole by a scalar field propagating on it and the boundary two-point Green function. We explore how positions inside the horizon are encoded in the boundary theory. The main idea is to compare two different semi-classical approximations of the Green function and see how this indicates the bulk-boundary relation. Writing the Green function in the Fourier integration of the momentum space correlation function, we can approximate it by the steepest descent method and the Green function is dominated by saddle points. Alternatively, writing the Green function in the form of the Feynman paths integration, we can apply the geodesic approximation and the Green function is dominated by certain geodesics joining the two points. To relate the two approximations, we deduce a geodesic approximation from the saddle point approximation by using a key observation of Festuccia and Liu, which is a frequency-geodesic identification, arising from comparing the WKB wave equation and the space-like geodesic equation. As an application, we find saddles of the Green function and hence their corresponding geodesics. The conclusion is that some of these geodesics do go inside the horizon. This gives the possibility of resolving the singularity from the boundary theory.

1 Introduction

Black hole singularities are interesting to study because they are beyond the scope of general relativity. Since classical geometry cannot give a clear explanation of these singularities, we therefore count on other available theories, like string theory, to search for answers. One way to gain understanding of the black hole singularities is using the AdS/CFT correspondence conjectured by Maldacena [1]. The conjecture is that string theory on $AdS_5 \times S^5$ corresponds to a conformal field theory on the boundary of the AdS_5 . More detailed matching of the two theories was worked out by Gubser, Klebanov, Polyakov [2] and Witten [3] by comparing spectra and correlation functions in the dual theories.

Based on this, Balasubramanian et.al. [4, 5] focused on how geometrical description of the bulk is manifested in the boundary theory. They described a variety of spacetime probes dynamically from the boundary perspective. To study dynamical properties, they provided a Hamiltonian framework of the AdS/CFT correspondence in the Lorentzian signature. It is essentially obtained from the Euclidean signature AdS/CFT correspondence by analytic continuation. The new feature of the Lorentzian signature correspondence is the appearance of normalizable modes in the bulk, rather than simply non-normalizable ones which appeared in the Euclidean signature. While the non-normalizable modes are mapped to the boundary act as sources coupled with dual boundary CFT operators, the normalizable modes, explained as physical low energy excitations of the bulk space time, are mapped to states comprising the Hilbert space of a given boundary Hamiltonian. Regarding the normalizable modes as probes on the bulk, the bulk and boundary states correspondence provides a dynamical description of the bulk from the perspective of the boundary. Banks, Douglas, Horowitz and Martinec [6] in the same angle provided a scheme to relate boundary operators to dynamical fields on the bulk. Klebanov and Witten in [7] calculated expectation values of boundary operator from the normalizable modes. In particular, two-point functions in the boundary CFT can be obtained by the limit of two-point functions in the bulk as the points are moved to the boundary of the spacetime. Our boundary two-point function calculation is based on this fact.

The matching of states between the bulk and the boundary implies that local operators on the boundary may contain information of the field on the bulk, which satisfies the holographic principle. Realisation of these ideas can be seen, for example: Keski-Vakkuri in [8] made an extension of the Lorentzian AdS/CFT from the AdS_3 [4] to the BTZ black hole. Danielsson et. al. [9] studied a non-trivial probe (a spherically collapsing matter) on the bulk through the boundary CFT. Even with the matching of states, we should say that it is still a hard problem to extract information inside the horizon of a AdS black hole from the boundary point of view. Works on this respect are initiated by for example by [10, 11], more recent attempts are as in [12, 13, 14, 15, 16, 17, 18, 19]. The

technical problem of identifying the bulk position from the boundary perspective becomes crucial. The geodesic approximation [13] is a favourite technique in this context. In the semi-classical limit, the CFT correlators can be represented in the form of Feynman paths integral of quantum mechanics, and the integration is dominated by certain geodesics. In this way, the geometric picture on the bulk appears. It is possible to probe singularities by studying the boundary objects which can be related to geodesics going inside the horizon. Works on this aspect are for example [12, 13, 17, 18].

In the same stream, Festuccia and Liu [20] studied the AdS_5 black hole singularity. They gave a method to match space-like geodesics in the bulk with momentum space Wightman functions of CFT operators in the semi-classical limit. As our present work on BTZ black holes heavily depends on their proposal, we will give a summary of their results. They considered a massive scalar field propagating on the bulk AdS_5 black hole and studied the Hartle-Hawking Green function. The position space correlation function can be mapped to the boundary correlation function through the AdS/CFT correspondence. To find correspondences between bulk positions and boundary states, they consider the semi-classical limit of the Green function. On one hand, the Green function, written as the Fourier integration of the momentum space Green function, can be approximated by the methods of steepest descent [21]. The integration is dominated by its evaluation at saddles. On the other hand, if we write the Green function in the Feynman paths integral of quantum mechanics, it can be approximated by the geodesic approximation. The key to relate the two approximations is the observation of a frequency-geodesic relation. After a precise analytic continuation procedure, the relation becomes a mathematically well-defined.

Mathematically, this frequency-geodesic relation gives the following interesting property: Firstly, real frequencies parametrize Euclidean time separation of geodesics and these geodesics are of real turning point outside the horizon. Secondly, purely imaginary frequencies parametrize Lorentzian time separation of geodesics and these geodesics are of real turning point inside the horizon. The position space Green function in terms of Fourier transformation has integration contour along real frequencies and saddles picked are near real axis, where the corresponding geodesics are with turning points outside the horizon. Festuccia and Liu in this regard proposed a new observable by replacing the contour by the purely imaginary axis. In this way, the saddles picked by the new observable are on the purely imaginary axis, and corresponding geodesics are with real turning point inside the horizon. Therefore, the new observable is able to carry signals from the singularity. Further, they suggested possible methods to resolve the singularity by using the new observable as an large N CFT object on the boundary. However, since the Klein-Gordon equation of modes on the AdS black hole background is hard to be solved exactly, the Green function does not have an exact formula. This makes it technically hard. We will apply their methods

on the BTZ black hole, where exact analytic solution is available.

Now we will give a summary of our work on the BTZ black hole. We choose our spacetime probe to be a massive scalar field described by the Klein-Gordon equation on the BTZ background and solve the equation exactly. By adding boundary conditions, we pick out normalizable modes according to the classification of modes in [8] in the framework of the Lorentzian signature AdS/CFT correspondence. As mentioned before, normalizable modes can be seen as fluctuations of the background and are mapped to states on the boundary, forming a Hilbert space. Here we are applying the argument in [4] directly without mentioning the specific choice of vacuum. Their description is actually set on the Poincaré vacuum and the analytic continuation of the AdS/CFT correspondence is consistent with this vacuum. However, how the description fits into other vacua is not very clear. Nevertheless, we would like to choose the Hartle-Hawking vacuum. Because of this, we fit ourselves in the pretty much equivalent framework of [6], [7] instead.

In the quantum field theory on a curved spacetime, a vacuum state can be defined by specific modes. Modes are decided by the chosen coordinates and boundary conditions. Such choices are preferred by the particular physical situation considered. Extensive discussion on choices of vacua can be found for example in [22]. The Hartle-Hawking vacuum is defined along with the discovery of the black hole radiation in [23]. The defining modes of this vacuum are the Kruskal modes and the Hartle-Hawking Green function can be obtained by a summation of Kruskal modes. Alternatively, the Hartle-Hawking Green function can be directly defined as analytic solution of some differential equation with specified boundary condition as boundedness at the future and past horizons [23]. There is another set of modes called the Bouliubov modes closely related to Kruskal modes [24]. The corresponding vacuum is called the Bouliubov vacuum. The Kruskal modes can be obtained from the Bouliubov modes by imposing boundary conditions on horizons and the corresponding vacua are related by a Bouliubov transformation [25]. Seen from an observer who takes the Bouliubov vacuum as vacuum, the Kruskal modes are in a thermal bath at the Hawking temperature. The analytic structure of the thermal Green function, which can be obtained by summation of Bouliubov modes at the Hawking temperature, agrees with that of the Hartle-Hawking Green function [26]. We obtain the Hartle-Hawking Green function on the BTZ black hole in this way. Through the AdS/CFT correspondence, the corresponding two-point Green function on the boundary can be obtained.

To see how the explicit boundary Green function encodes bulk dynamics, we take the semi-classical limit to arrive at a frequency-geodesic relation as in [20] and deduce a geodesic approximation from the saddle point approximation. This can be explained in the following way. Consider this scalar field propagating on the BTZ black hole and its two-point function with the two points A and B

inserted on distinct boundaries in the Penrose diagram. Taking semi-classical limit, it can be seen as a wavepacket propagating along geodesics. This can also be explained as in the Feynman path integration of quantum mechanics, where dominant terms are certain geodesics joining A and B . It is plausible to make a term by term identification of the WKB approximation of the wave equation and the geodesic equation, both appearing as equations of motions in the semi-classical limit. After proper analytic continuation procedure, this identification gives a definite mapping between frequencies (saddles) and geodesics. Hence a geodesic approximation can be deduced from the properties of saddles. We obtain similar properties of the frequency-geodesic relation as appeared in the AdS_5 black hole and find out that some geodesics have turning points inside the horizon. Further, if we analogously deform the integration contour from the real axis to the imaginary axis we get a new function, assuming that a regularization of the function exists. Saddles of the new function correspond to those geodesics with real turning point infinitely closed to the singularity. In this sense, we find signatures of the singularity on the bulk in the boundary correlation function. We should make two remarks regarding the above method: First of all, this is by no means the only way to make a geodesic approximation. For example different analytic procedure can lead to different dominating geodesics, while the correlation function remains the same. This kind of argument was made by Kraus, et. al. in [16]. They analytically continued the correlation function directly in two different procedures but yield the same physical amplitude. Secondly, the frequency-geodesic relation does not have physical meaning beyond the semi-classical limit. The reason is that the validity of this relation is supported by the principle of wave-particle duality. This is only meaningful in the semi-classical limit. For example, for a frequency which is not at saddle point, the corresponding geodesic may not join the two points in the two-point function.

The plan for the rest of the paper is as follows. Section two will give a summary of the BTZ metric and space-like geodesics on it. In section three, we will solve the Klein-Gordon equation on the BTZ metric explicitly and find normalizable modes. Then we write down the Hartle-Hawking Green function by summation of these modes at the Hawking temperature of the black hole and get the correlation function in the boundary theory by the AdS/CFT correspondence. Section four gives the explicit mapping between geodesics and saddles on the BTZ black hole at the semi-classical limit. We will first give a proof of the relation formally and then provide an explicit procedure of analytic continuation to make it well-defined so that we obtain a geodesic approximation of the Green function. Section five is an application of this geodesic approximation. By the explicit correlation function, we can find saddles and their corresponding geodesics. Finally we draw some conclusions.

2 The BTZ geometry

We will summarise the construction of the BTZ black hole and write down the space-like geodesic equations, the proper length, the proper time and the proper displacement in the angular direction.

2.1 The BTZ metric

We will sketch the construction the BTZ black hole of Banados, Henneaux, Teitelboim and Zanelli [27] in the non-rotating case. Roughly speaking, the BTZ black hole metric is obtained as a quotient metric from the AdS_3 metric. The AdS_3 space is defined in terms of its embedding in a four dimensional flat space of signature $(- - ++)$:

$$ds_{\mathbb{R}^{2,2}}^2 = -du^2 - dv^2 + dx^2 + dy^2$$

through the equation $-v^2 - u^2 + x^2 + y^2 = -l^2$. We will assume $l = 1$ from now on. We change coordinates from (u, v, x, y) to (μ, t, x, y) by

$$u = \cosh \mu \sin t, \quad v = \cosh \mu \cos t,$$

where $0 \leq \mu < \infty$ and $0 \leq t < 2\pi$. The new coordinates are defined on the whole of AdS_3 . Changing the coordinates (x, y) into polar coordinates,

$$x = \sinh \mu \cos \theta, \quad y = \sinh \mu \sin \theta.$$

The resulting metric is

$$ds_{AdS_3}^2 = -\cosh^2 \mu dt^2 + d\mu^2 + \sinh^2 \mu d\theta^2.$$

Observe that the periodicity of t implies the existence of closed time-like curves. To avoid this, t is unwrapped by requiring $t \neq t + 2\pi$. In other words, we are considering a universal covering space of the AdS_3 , denoted by $CAdS_3$, with metric

$$ds_{CAdS_3}^2 = -(r^2 + 1)dt^2 + \frac{1}{r^2 + 1}dr^2 + r^2 d\theta^2,$$

where $r = \sinh \mu$.

By construction, $CAdS_3$ has $SO(2, 2)$ as its isometry group. The BTZ black hole metric will be obtained from the quotient metric of $CAdS_3$ by certain discrete isometry subgroup of the $SO(2, 2)$. In general, if ξ is a Killing vector on the spacetime, the transformation from any point P to $\exp(s\xi)P$ in $CAdS_3$ is an isometry. The group $\{\exp(s\xi) : s \in \mathbb{R}\}$ is an isometry group parametrised by s . If s is restricted to $s = 2\pi n$ for $n \in \mathbb{Z}$, then it parametrises a discrete subgroup. We call it $\Xi(\xi)$. The quotient space $CAdS_3/\Xi(\xi)$ inherits a quotient metric

from $CAdS_3$. Under the coordinates (u, v, x, y) , it is proposed that the Killing vector $\xi = r_+ \left(u \frac{\partial}{\partial v} - v \frac{\partial}{\partial u} \right)$ up to an isometric transformation. The BTZ metric is defined to be the quotient metric induced from $CAdS_3$ through the discrete isometry subgroup $\Xi(\xi)$. However, to exclude time-like curves on the quotient metric, $\xi \cdot \xi > 0$ needs to be satisfied everywhere on the spacetime. Hence the final BTZ black hole spacetime is defined to be the BTZ metric on the region where $\xi \cdot \xi > 0$. These regions can be divided into an infinite number of regions of two different types.

1. Region of type I, $r_+^2 < \xi \cdot \xi < \infty$ (the outer region).
2. Region of type II, $0 < \xi \cdot \xi < r_+^2$ (the inner region).

We restrict to two continuous regions of both types and introduce the coordinates (t, r, ϕ) as follows,

1. Region I: $r_+ < r$,

$$u = \frac{r}{r_+} \cosh r_+ \phi, \quad v = \frac{\sqrt{r^2 - r_+^2}}{r_+} \sinh r_+ t,$$

$$x = \frac{r}{r_+} \sinh r_+ \phi, \quad y = \frac{\sqrt{r^2 - r_+^2}}{r_+} \cosh r_+ t.$$

2. Region II: $r < r_+$,

$$u = \frac{r}{r_+} \cosh r_+ \phi, \quad v = -\frac{\sqrt{-r^2 + r_+^2}}{r_+} \cosh r_+ t,$$

$$x = \frac{r}{r_+} \sinh r_+ \phi, \quad y = -\frac{\sqrt{-r^2 + r_+^2}}{r_+} \sinh r_+ t.$$

In the coordinates (t, r, ϕ) , the Killing vector is $\xi = \frac{\partial}{\partial \phi}$ and the discrete subgroup acts as taking the identification $\phi = \phi + 2n\pi$, for $n \in \mathbb{Z}$. The BTZ black hole metric is thus the quotient metric by the isometry discrete subgroup generated by ξ on the region where $\xi \cdot \xi > 0$,

$$ds_{BTZ}^2 = -(r^2 - r_+^2)dt^2 + \frac{1}{r^2 - r_+^2}dr^2 + r^2d\phi^2 \quad (1)$$

with the identification $\phi = \phi + 2n\pi$, $n \in \mathbb{Z}$. We will assume $r_+ = 1$ from now on.

2.2 Geodesics on the BTZ black hole

On the BTZ metric (1), there are two particular Killing vectors, $\partial_t = (1, 0, 0)$ and $\partial_\phi = (0, 0, 1)$. Their corresponding conserved quantities are energy E^2 and angular momentum L^2 . Since energy and angular momentum are conserved on geodesics, we can write down geodesic equations in terms of E and L . Let $\vec{x}(\lambda) = (t(\lambda), r(\lambda), \phi(\lambda))$ be a space-like geodesic with the affine parameter λ . Its geodesic equation can be written as

$$\frac{1}{r^2 - 1} \left(\frac{dr}{d\lambda} \right)^2 + \frac{L^2}{r^2} - \frac{E^2}{r^2 - 1} = 1, \quad (2)$$

where $E = (r^2 - 1) \frac{dt}{d\lambda}$ and $L = r^2 \frac{d\phi}{d\lambda}$. If we define an effective potential by

$$V_{eff} = -(r^2 - 1) \left(1 - \frac{L^2}{r^2} \right), \quad (3)$$

then (2) gives $\left(\frac{dr}{d\lambda} \right)^2 = E^2 - V_{eff}$. This can be thought of as the equation of motion of a particle of energy E^2 in a potential V_{eff} . Observe that the potential (3) behaves differently according to the different values of L . See Fig. 1. Imagine

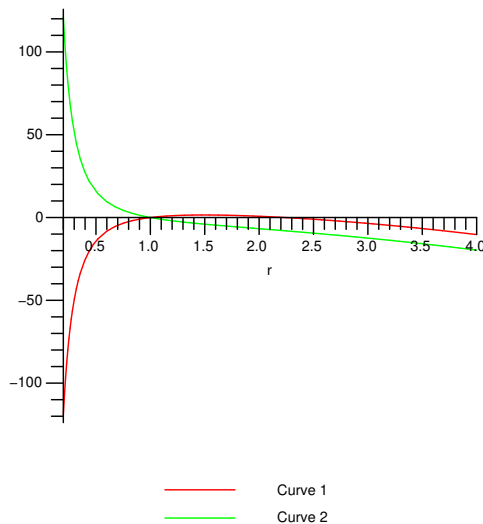


Figure 1: Potential v.s. radius with different L .

a particle of energy E^2 coming from boundary towards the singularity. When L is a real number, the potential is represented by the Curve 1 of Fig. 1. We can see that with big enough E^2 , the particle will go inside the horizon and be trapped there. However, when L is a purely imaginary number, the potential is represented by the Curve 2. We can see that no matter how big E^2 is, the particle

has to bounce back. When E^2 is infinitely large, the turning point of the geodesic becomes infinitely closed to the singularity. In this case, the returned particle may carry signatures of the singularity. Therefore, we want to consider the case when L is a purely imaginary number. For simplicity, we assume $L = iL_I$ for $L_I > 0$. The turning point r_c of such particles can be solved as solutions of the equation

$$E^2 + r^2 - L^2 - 1 + \frac{L^2}{r^2} = 0. \quad (4)$$

The proper time \mathfrak{t} , proper length \mathfrak{l} and proper angular displacement \mathfrak{d} of a space-like geodesic with energy E^2 and angular momentum L^2 are as follows,

$$\mathfrak{t}(E, L) = 2 \int_{r_c}^{\infty} \frac{E}{(r^2 - 1)\sqrt{E^2 + (r^2 - 1)(1 - \frac{L^2}{r^2})}} dr \quad (5)$$

$$\mathfrak{l}(E, L) = 2 \int_{r_c}^{\infty} \frac{1}{\sqrt{E^2 + (r^2 - 1)(1 - \frac{L^2}{r^2})}} dr \quad (6)$$

$$\mathfrak{d}(E, L) = 2 \int_{r_c}^{\infty} \frac{L}{r^2 \sqrt{E^2 + (r^2 - 1)(1 - \frac{L^2}{r^2})}} dr, \quad (7)$$

where the integrations are all over the contour along the real r axis from r_c to positive infinity.

3 Correlation functions on the BTZ black hole

We will look for the exact solution of a massive scalar field described by the Klein-Gordon equation on the BTZ metric and then pick out a set of normalizable modes satisfying the reflective boundary condition mentioned in reference [24]. These modes are the Boulware modes and the vacuum defined by them are the Boulware vacuum. In the same reference, Hemming and Keski-Vakkuri constructed the Kruskal modes out of these normalizable modes. They first make linear combinations of the Boulware modes in general and then pick out the Kruskal modes by imposing the analytic condition on the horizon. The Kruskal modes are the modes which define the Hartle-Hawking vacuum. The Hartle-Hawking Green function agrees with the thermal Boulware Green function at the Hawking temperature [26]. We obtain the latter by summing the Boulware modes. Applying the AdS/CFT correspondence, the boundary two-point function can be obtained from the bulk two-point function by taking points to the boundary [6, 7].

3.1 The AdS/CFT correspondence

We will illustrate the relevant parts of the AdS/CFT correspondence in more detail, and specify our footing in the AdS/CFT picture. While the original AdS/CFT correspondence is proposed for the Euclidean signature, the Hamiltonian framework of the AdS/CFT correspondence constructed by Balasubramanian et. al. in [4, 5] is in the Lorentzian signature. We will explain the new features which appeared in the Lorentzian signature through the simple example of a scalar field of mass m propagating on the bulk AdS_{d+1} . Note that d is the dimension of the boundary spacetime. The basic formula from the AdS/CFT correspondence in the Euclidean signature [3] is

$$Z(\Phi) = \exp(-S(\Phi)) = \langle \exp\left(\int_B \Phi_0 \mathcal{O}\right) \rangle,$$

where $S(\Phi) = \frac{1}{2} \int d^{d+1}x \sqrt{g}(|d\Phi|^2 + m^2\Phi^2)$ is the effective action as a function of the bulk field Φ , Φ_0 is the boundary limit of Φ up to a radial scaling and \mathcal{O} is the dual operator in the CFT. This can be understood as saying that boundary conditions for the bulk theory are dual to sources on the boundary theory. It can be shown that, under the requirement of regularity of the solution, for a given boundary field Φ_0 in the bulk, there exists a unique solution Φ on the bulk which has the boundary limit Φ_0 . Its limit is given as $\Phi(z, x) = z^{2h_-} \Phi_0(x)$ where z is a radial coordinate with $z \rightarrow 0$ around the boundary, x is the coordinate on the boundary and $h_- = \frac{d}{4} - \frac{\sqrt{d^2+4m^2}}{4}$. Explicitly,

$$\Phi(z, x) = c \int d^d x' \frac{z^{2h_+}}{(z^2 + |x - x'|^2)^{2h_+}} \Phi_0(x'), \quad (8)$$

where $h_+ = \frac{d}{4} + \frac{\sqrt{d^2+4m^2}}{4}$. There is a subleading normalizable component of Φ with boundary behaviour $z^{2h_+} \tilde{\Phi}(x)$ for some $\tilde{\Phi}(x)$. Further, the expectation value of the corresponding operator $\mathcal{O}(x)$ dual to $\Phi(z, x)$ can be evaluated as $\tilde{\Phi}$, i.e.

$$\langle \mathcal{O}(x) \rangle_{\Phi_0(x)} = \langle \mathcal{O}(x) \exp(\Phi_0(x)\mathcal{O}(x)) \rangle \sim 2h_+ \tilde{\Phi}(x). \quad (9)$$

The new feature of the Lorentzian signature is that the bulk wave function admits normalizable mode solutions as well as non-normalizable modes. By analytic continuation of a bulk-boundary operator, a general non-singular solution on the bulk with boundary limit $z^{2h_-} \Phi_0(x)$ is now given as summation of the unique $\Phi(z, x)$ obtained in the Euclidean signature and normalizable modes $\Phi_n(z, x)$. Such modes describe the physical low energy excitations of the spacetime and they behave as $z^{2h_+} \tilde{\Phi}_n(x)$ for some $\tilde{\Phi}_n(x)$ near the boundary. The regular solution is explicitly,

$$\Phi(z, x) = \Phi_n(z, x) + c \int d^d x' \frac{z^{2h_+}}{(z^2 + |x - x'|^2)^{2h_+}} \Phi_0(x')$$

Comparing with (8), Φ_n 's are new. The expectation value of the dual operator $\mathcal{O}(x)$ in the presence of normalizable modes can be evaluated as

$$\langle \tilde{\Phi}_n(x) | \mathcal{O}(x) | \tilde{\Phi}_n(x) \rangle_{\Phi_0(x)} \sim 2h_+ \tilde{\Phi}_n(x) + 2h_- \tilde{\Phi}(x),$$

Comparing with (9), the contribution of the first term from excited states is new. To see the dynamical effect, it suffices only to consider the contribution from the first term while turning off the source term. We are working under this assumption and consider only normalizable modes Φ_n 's. In particular, the boundary two-point function $\tilde{G}(x, x')$ under this framework is obtained by simply taking the two points in the bulk two-point function $G((z, x), (z', x'))$ to the boundary up to a scaling in the radial direction [7],

$$\tilde{G}(x, x') = \lim_{z, z' \rightarrow 0} z^{-2h_+} z'^{-2h_+} G((z, x), (z', x')). \quad (10)$$

Our computation of two-point functions on the boundary is based on these facts.

3.2 The exact solution of the radial part of the KG equation

In the following, we will find the normalizable modes Φ_n mentioned above for a scalar field on our BTZ black hole. The Klein-Gordon equation of a free scalar field $\Phi(r, t, \phi)$ propagating on the BTZ metric (1) is given as

$$\square \Phi = m^2 \Phi, \quad (11)$$

where \square is the Laplace-Beltrami operator defined by the metric. We can solve this equation by the method of separation of variables. Write

$$\Phi(t, r, \phi) = \sum_{\omega, J} \exp(iJ\phi) \exp(-i\omega t) r^{-1/2} X(r).$$

The radial part of the equation of motion is

$$-(r^2 - 1)^2 \frac{d^2 X(r)}{dr^2} - 2r(r^2 - 1) \frac{dX(r)}{dr} - \omega^2 X(r) + V(r)X(r) = 0, \quad (12)$$

where

$$V(r) = (r^2 - 1) \left(\frac{J^2 + \frac{1}{4}}{r^2} + \nu^2 - \frac{1}{4} \right), \quad \nu^2 = 1 + m^2.$$

Related to terms in Section 3.1, we have $d = 2$ and $h_{\pm} = \frac{1 \pm \nu}{2}$. Equation (12) can be found in terms of hypergeometric functions,

$$X(r) = r^{\frac{1}{2}} (1 - r^2)^{-\frac{i\omega}{2}} (C_1 r^{-iJ} G(r) + C_2 r^{iJ} H(r)), \quad (13)$$

where

$$G(r) = F\left(\frac{-i\omega - iJ - \nu + 1}{2}, \frac{-i\omega - iJ + \nu + 1}{2}; 1 - iJ, r^2\right),$$

$$H(r) = F\left(\frac{-i\omega + iJ - \nu + 1}{2}, \frac{-i\omega + iJ + \nu + 1}{2}; 1 + iJ, r^2\right)$$

and C_1, C_2 are constants. We want to pick out the normalizable modes satisfying the reflective boundary condition [24] as follows:

$$X(z) \longrightarrow \begin{cases} \exp(i\omega z) \exp(i\delta) + \exp(-i\omega z) \exp(-i\delta) & \text{as } z \longrightarrow \infty \quad (\text{horizon}) \\ C(\omega, J) z^{\frac{1}{2} + \nu} & \text{as } z \longrightarrow 0 \quad (\text{boundary}) \end{cases}, \quad (14)$$

where δ is some real constant and the coordinate z is defined by

$$z(r) = \frac{1}{2} \ln \frac{r+1}{r-1}.$$

With these boundary conditions, we are able to fix constants C_1 and C_2 . Since the computation is lengthy, we will refer the reader to Appendix for details. The resulting fixed constants in particular give us

$$C(\omega, J)^2 = \frac{\exp(\pi\omega)(\exp(2\pi\omega) - 1)\omega}{2\pi\Gamma(1 + \nu)^2} \quad (15)$$

$$\Gamma\left(\frac{1}{2}(i\omega + iJ + \nu + 1)\right)\Gamma\left(\frac{1}{2}(-i\omega + iJ + \nu + 1)\right)$$

$$\Gamma\left(\frac{1}{2}(i\omega - iJ + \nu + 1)\right)\Gamma\left(\frac{1}{2}(-i\omega - iJ + \nu + 1)\right)$$

at boundary¹, which will be used.

3.3 Correlation functions

The Hartle-Hawking Green function agrees with the thermal Green function of the normalizable modes as in (14) at the Hawking temperature. At zero temperature, the Wightman function is given by the modes sum,

$$G^+((t, r, \phi), (t', r', \phi')) = \langle 0 | \Phi(t, r, \phi) \Phi(t', r', \phi') | 0 \rangle$$

$$= \sum_{\omega, J} \exp(iJ(\phi' - \phi) - i\omega(t' - t)) r^{-1/2} r'^{-1/2} X(r) X(r').$$

Since ω and J are not quantized under the boundary condition (14), we can write the summation in the integration form,

$$G^+((t, r, \phi), (t', r', \phi')) = \int_{-\infty}^{\infty} d\omega \int_{-\infty}^{\infty} dJ [\exp(iJ(\phi' - \phi) - i\omega(t' - t)) r^{-1/2} r'^{-1/2} X(r) X(r')].$$

¹ This constant is worked out with the help of Mukund Rangamani.

On the other hand, the Fourier integration representation of $G^+((t, r, \phi), (t', r', \phi'))$ is

$$G^+((t, r, \phi), (t', r', \phi')) = \int_{-\infty}^{\infty} d\omega \int_{-\infty}^{\infty} dJ [\exp(iJ(\phi' - \phi) - i\omega(t' - t)) \mathcal{G}^+(\omega, J; r, r')].$$

Comparing coefficients in the two integrations above, the Wightman function in the momentum space is

$$\mathcal{G}^+(\omega, J; r, r') = r^{-1/2} r'^{-1/2} X(r) X(r'). \quad (16)$$

The Wightman function $\mathcal{G}_\beta^+(\omega, J; r, r')$ at the Hawking temperature $T_H = \frac{1}{\beta}$, where $\beta = 2\pi$, can be obtained from the Wightman function at the zero temperature by [28],

$$\mathcal{G}_\beta^+(\omega, J; r, r') = \frac{\mathcal{G}^+(\omega, J; r, r')}{1 - \exp(-\beta\omega)} = \frac{\exp(\beta\omega)}{\exp(\beta\omega) - 1} r^{-1/2} r'^{-1/2} X(r) X(r').$$

This is the momentum space Hartle-Hawking Green function. We can pass the AdS/CFT correspondence (10) to the momentum space, the boundary Green function can be obtained as,

$$\begin{aligned} \tilde{\mathcal{G}}_\beta^+(\omega, J) &= \lim_{r, r' \rightarrow \infty} r^{2h} r'^{2h} \mathcal{G}_\beta^+(\omega, J; r, r') \\ &= \lim_{r, r' \rightarrow \infty} r^{1+\nu} r'^{1+\nu} \frac{\exp(\beta\omega)}{\exp(\beta\omega) - 1} r^{-1/2} r'^{-1/2} C(\omega, J)^2 z^{1/2+\nu} z'^{1/2+\nu} \\ &= \frac{\exp(\beta\omega)}{\exp(\beta\omega) - 1} C(\omega, J)^2. \end{aligned}$$

Substituting (15) in, we obtained the boundary thermal Green function in the momentum space,

$$\begin{aligned} \tilde{\mathcal{G}}_\beta^+(\omega, J) &= \frac{\exp(3\pi\omega)\omega}{2\pi\Gamma(1+\nu)^2} \Gamma\left(\frac{1}{2}(i\omega + iJ + \nu + 1)\right) \Gamma\left(\frac{1}{2}(-i\omega + iJ + \nu + 1)\right) \\ &\quad \Gamma\left(\frac{1}{2}(i\omega - iJ + \nu + 1)\right) \Gamma\left(\frac{1}{2}(-i\omega - iJ + \nu + 1)\right). \end{aligned} \quad (17)$$

To analytically continue this function by extending the domain of ω from the real line to the complex ω -plane, we need to identify singular points of $\tilde{\mathcal{G}}_\beta^+(\omega, J)$. They are located at

$$\{\omega = \pm J \pm (1 - \nu)i \mp 2Ni\} \cup \{\omega = \pm J \mp (1 - \nu)i \pm 2Ni\}, \quad (18)$$

where N is any positive integer. For later use, we change the scale of variables as $u = \frac{\omega}{\nu}$ and $k = \frac{J}{\nu}$ and further assume that k is a positive real number. This

assumption will be made clear later by relating it to the assumption of $L = iL_I$ where $L_I > 0$ in Section 2.2. Singular points (18) in the large ν limit are located at

$$\{u = \pm k \pm i \pm 2ni\} \cup \{u = \pm k \mp i \mp 2ni\}, \quad (19)$$

where $n = N/\nu$ and N is any positive integer. On the complex u -plane, the

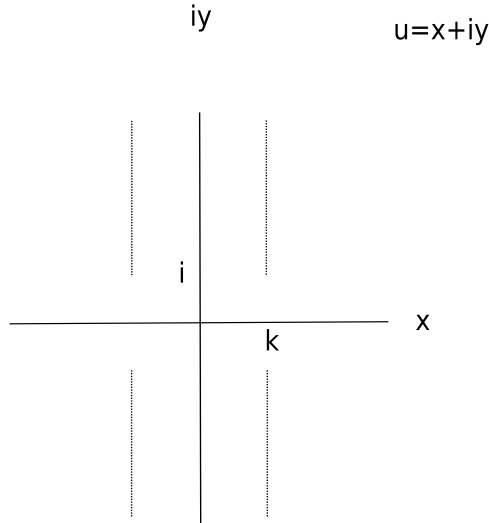


Figure 2: Poles of $\tilde{\mathcal{G}}_{\beta}^{+}(u, k)$ in the large ν limit.

distance between poles become very small as $\nu \rightarrow \infty$ and the four lines of poles become branch cuts. This is illustrated in Fig. 2. These are the branch cuts for analytical continuation of $\tilde{\mathcal{G}}_{\beta}^{+}(u, k)$.

4 Correlation functions and geodesics on the BTZ black hole

We want to see how the exact boundary correlation function probe the bulk geometry. The main idea is to relate correlation functions to geodesics on the bulk. To achieve this, we consider two different semi-classical approximations of the two-point Green function. The first method is the geodesic approximation. Indeed, wavepackets propagate like particles along geodesics in the semi-classical limit. With respect to the decomposition of complex time separation into the Lorentzian and Euclidean sections, i.e. $t+i\tau$, the BTZ spacetime can be projected onto the two sections as shown in Fig. 3. We are interested in the case when the two points are inserted on distinct boundaries of the Penrose diagram, describing the Lorentzian section of the spacetime. Geodesics joining distinct boundaries are like A , B , C and D in Fig. 3 (a). The second approach is by the steepest

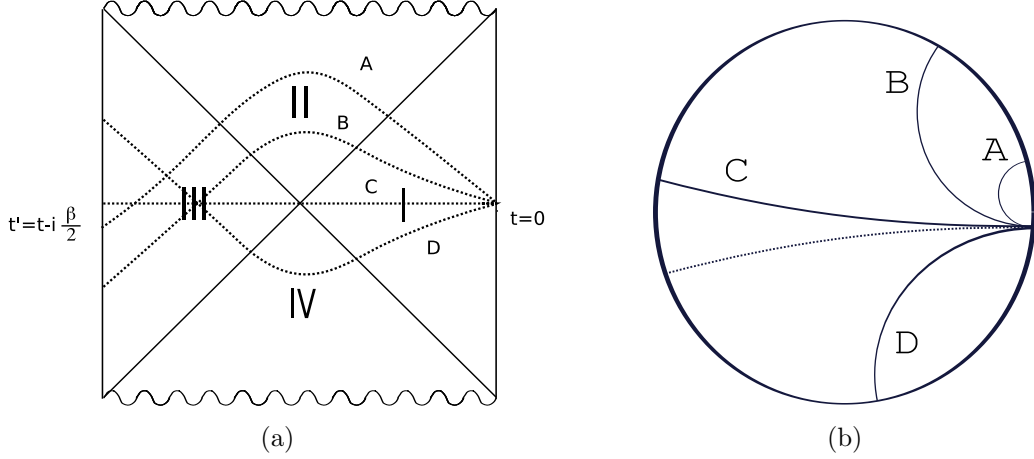


Figure 3: (a) Space-like geodesics joining points on distinct boundaries with time separation $t' - t - i\frac{\beta}{2}$ in the Lorentzian section of the spacetime. Lines of equal Lorentzian time are straight lines through the centre, the time being given by the slope. Lines of equal radius r are hyperbolas in each region (not shown), with asymptotics at the cross in the middle. The upper and lower waved lines are the future and past singularities. The upper part of the cross is the future horizon $r = 1$ and the lower part of the cross is the past horizon. The left and right straight lines are two distinct boundaries at $r = \infty$. Each wedge is associated with a constant Euclidean time. Region I is of time 0, region II is of time $-i\frac{\beta}{4}$, region III is of time $-i\frac{\beta}{2}$ and region IV is of time $-i\frac{3\beta}{4}$. The jumping of $-i\frac{\beta}{4}$ comes from the fact that integration of proper time from one region to the next picks up a pole at the horizon with a factor of $-i\frac{\beta}{4}$. A, B, C and D all have Euclidean time separation $-\frac{\beta}{2}$. As u varies from $-i\infty$ to 0 along the imaginary axis, geodesic moves from A to B and then to C . Geodesic D corresponds to $u_I > 0$. (b) Space-like geodesics in the Euclidean section. The radial direction of the spacetime is along the radial direction of the circle. The centre of the circle is chosen to be at the horizon, $r = 1$ and the boundary of circle is where $r = \infty$. The Euclidean time τ is in the angular direction with period 2π . As u varies from $+\infty$ to 0^+ , the corresponding geodesic changes from A to B , and then to C . Note that C turns back before it reaches the horizon at the centre. Geodesic D stands for a geodesic with $u < 0$.

descent method to evaluate the correlation function as Fourier integration of the momentum space Green function. For points inserted on distinct boundaries in the Lorentzian section space-time, the boundary two-point function can be obtained from the Wightman functions by changing the time variable from t' to $t' - i\frac{\beta}{2}$. That is,

$$\tilde{G}_{12}(t, t'; k) = \int_{-\infty}^{\infty} \exp(-i\nu u(t' - t - i\frac{\beta}{2})) \tilde{\mathcal{G}}_{\beta}^{+}(u, k). \quad (20)$$

The asymptotic expansion of the integration is dominated by saddle points. The goal is to relate the saddles and the geodesics, both appeared as dominating objects in the semi-classical limit, so that we can deduce a geodesic approximation from the saddle point approximation. In other words, we want to make the following geodesic approximation explicitly defined in the semi-classical limit,

$$\tilde{G}_{12}(t, t'; k) = \sum_i \exp(-m(l_i + f_i(k))), \quad (21)$$

where i indicates different dominant geodesics, m is the mass of the scalar field and l_i is proper length of the i -th dominant geodesic joining the two points and $f_i(k)$ is a function indicating the contribution from the angular momentum k . We will firstly sketch the method of steepest descent, secondly provide a formal proof of (21) and finally deduce an explicit geodesic approximation.

4.1 The steepest descent methods

We will briefly summarise the steepest descent methods from [21, 29]. It is a technique to get asymptotic expansions at the large ν for integrations in the form,

$$I(\nu) = \int_C g(u) \exp(\nu h(u)) du, \quad (22)$$

where C is a contour on the complex u -plane, and $g(u)$ and $h(u)$ are holomorphic functions. The points of u -plane where $\frac{dh(u)}{du} = 0$ are called *saddle points*. They are saddle points on the real surface representing $|\exp(\nu h(u))|$, which is seen as a function of the two real variables x and y with $x = \text{Re}(u)$, $y = \text{Im}(u)$. Curves along which $\text{Im}(\nu h(u))$ is constant are called *steepest descent paths*. Along such curves, $|\exp(\nu h(u))|$ changes as rapidly as possible. In other words, they are the gradient lines of $|\exp(\nu h(u))|$. The saddle point is a stationary point of the function $|\exp(\nu h(u))|$ along the steepest descent path. The method of steepest descents consists in deforming the path of integration C so as to make it coincide as far as possible with arcs of steepest paths. In this way, the integration is transformed to a real integration of the Laplacian type and the Laplace method may be used to evaluate the integral asymptotically. We summarise the methods in the following steps:

1. Identify the saddle points u_0 as zeros of $\frac{dh(u)}{du} = 0$.
2. Determine degree n of saddle point u_0 such that

$$\frac{d^q h(u)}{du^q} \Big|_{u_0} = 0, \quad q = 1, 2, \dots, n-1, \quad \frac{d^n h(u)}{du^n} \Big|_{u=u_0} = a \exp(i\alpha), \quad a > 0$$

for some real number α .

3. Determine directions of steepest descent of each saddle point: If $u - u_0 = \rho \exp(i\theta)$, then the steepest descent and the steepest ascent direction are given as

<i>Direction of</i>	θ
Steepest Descent	$-\frac{\alpha}{n} + \frac{(2p+1)\pi}{n} \quad p = 0, 1, \dots, n-1$
Steepest Ascent	$-\frac{\alpha}{n} + \frac{2p\pi}{n} \quad p = 0, 1, \dots, n-1$

4. Justify, via Cauchy's integral theorem, the deformation of the original contour of integration C onto one or more of the paths of steepest descent.
5. Determine the asymptotic expansions of the deformed integrals through Laplace methods.

For our interests of finding dominating saddles and eventually their corresponding geodesics, we do not need to go through the fifth step. The rest of the steps listed will become clearer when we consider our particular examples.

4.2 Saddle points and the geodesic approximation I

We will formally deduce (21) for now and provide a mathematically explicit description in the next subsection. Consider the Fourier integration of the two-point function (20) in the large ν limit,

$$\tilde{G}_{12}(t, t'; k) = \int_{-\infty}^{\infty} du \exp(-i\nu\nu(\Delta t - i\frac{\beta}{2})) \exp(2\nu Z(u, k)), \quad (23)$$

where $\Delta t = t' - t$ and we write $\tilde{\mathcal{G}}_{\beta}^{+}(u, k) = \exp(\nu Z(u, k))$ for some $Z(u, k)$ so that the Fourier integration is transformed into the form of (22). We can analytically continue the function $\tilde{\mathcal{G}}_{\beta}^{+}(u, k)$ from the real u -axis to the complex u -plane without difficulty by branch cutting pole lines illustrated in Fig. 2. Complex saddles can thus be obtained by solving the saddle point equation. The evaluation of the integrand at the dominating saddles is dominant in the asymptotic expansion of 20. On the other hand, we can use the language of Feynman paths integration of quantum mechanics for (23) in the semi-classical limit. There will be certain

geodesics joining the two points to dominate the integration in the spirit of wave-particle duality. Since the saddles and geodesics appear respectively as dominant terms in two different semi-classical approximations of the same correlation functions, we want to make a link between them. The first attempt is to simply make a term by term identification, by comparing units, between the wave equation and the geodesic equation [20].

To obtain the wave equation in the semi-classical limit, we use the ansatz $X(z) = \exp(\nu S(z))$ for the radial part of the Klein-Gordon field. Equation (12) can thus be written in terms of $S(z)$. We substitute in the expansion $S(z) = S_0(z) + \frac{1}{\nu}S_1(z) + \frac{1}{\nu^2}S_2(z) + \dots$, in which the $S_0(z)$ will be the leading term in the large ν limit. The radial part of the Klein-Gordon equation can further be written in terms of $S_0(z)$,

$$\frac{1}{r^2 - 1} \left(\frac{dS_0(z)}{dz} \right)^2 - \frac{k^2}{r^2} + \frac{1}{r^2 - 1} u^2 = 1. \quad (24)$$

On the other hand, recall the geodesic equation (2), describing space-like geodesics joining points on the boundary of energy E^2 and angular momentum L^2 . The assumption of equivalence between equations (24) and (2) suggests the following identification:

$$\frac{dS_0}{dz} \longleftrightarrow \frac{dr}{d\lambda}, \quad k \longleftrightarrow iL, \quad u \longleftrightarrow iE. \quad (25)$$

Observe that the relation between L and k is consistent with the assumptions that $L = iL_I$ for $L_I > 0$ and that k is positive.

Now we will show that (25) implies the formalism of the geodesic approximation of propagators as in (21). Write the momentum space Green function in terms of $S_0(z)$, i.e.,

$$\tilde{\mathcal{G}}_\beta^+(u, k) = \lim_{r, r' \rightarrow \infty} r^{1+\nu} r'^{1+\nu} \frac{\exp(\beta\omega)}{\exp(\beta\omega) - 1} r^{-1/2} r'^{-1/2} \exp(\nu S_0(z)) \exp(\nu S_0(z')) + \dots \quad (26)$$

and define $Z_0(u, k) = \lim_{z(r) \rightarrow 0} S_0(z)$. The semi-classical approximation of momentum space Green function is thus $\tilde{\mathcal{G}}_\beta^+(u, k) \sim \exp(2\nu Z_0(u, k))$ where $\nu \gg 1$. We apply the identification (25) and change coordinates from z to r in the integration. We obtain

$$\begin{aligned} Z_0(u, k) &\doteq \lim_{r \rightarrow \infty} \int_{z(r_c)}^{z(r)} \frac{dS_0}{dz} dz \\ &\doteq \lim_{r \rightarrow \infty} \int_{z(r_c)}^{z(r)} \sqrt{(r^2 - 1) \left(1 + \frac{k^2}{r^2} - u^2 \right)} dz \\ &\doteq iu \cdot \frac{1}{2} \mathbf{t}(u, k) - \frac{1}{2} \mathbf{l}(u, k) + \frac{1}{2} L \mathbf{d}(u, k), \end{aligned} \quad (27)$$

where r_c is the solution of

$$-\frac{k^2}{r^2} + \frac{1}{r^2 - 1}u^2 = 1 \quad (28)$$

and \mathbf{t} , \mathbf{l} , \mathbf{d} are from (5), (6) and (7), respectively. Also notice that equation (28) agrees with equation (4) under the assumption (25). Here “ \doteq ” reminds us that these are formal equalities. We will fix an analytic continuation procedure to make these equalities exact later. We make some immediate remark regarding (27). It implies that

$$\frac{2\partial Z_0(u, k)}{\partial(-iu)} = -\mathbf{t}(u, k), \quad \frac{2\partial Z_0(u, k)}{\partial(-ik)} = \mathbf{d}(u, k).$$

If we regard the proper length $\mathbf{l}(\mathbf{t}, \mathbf{d})$ as a function of (\mathbf{t}, \mathbf{d}) instead of (u, k) , then the above identities imply that $2Z_0(u, k)$ and $\mathbf{l}(\mathbf{t}, \mathbf{d})$ are related by a Legendre transformation. Geometrically, a Legendre transformation maps the graph of a function to the family of tangents to the graph. In our case, if the graph is $\mathbf{l}(\mathbf{t}, \mathbf{d})$ then the tangents are $\frac{d\mathbf{l}(\mathbf{t}, \mathbf{d})}{d\mathbf{t}} = iu$. Alternatively, if the graph is $2Z_0(u, k)$ then the tangents are $\frac{2dZ_0(u, k)}{du} = -it$. As Lagrangian and Hamiltonian we have the mathematical relation

$$2Z_0(u, k) + \mathbf{l}(\mathbf{t}, \mathbf{d}) = iut - ikd \quad (29)$$

and hence

$$\frac{d2Z_0(u, k)}{du} = it. \quad (30)$$

We further consider the decomposition of the identification $-iu = (r^2 - 1)\frac{d\lambda}{d\lambda}$ into the real and imaginary parts, and take integration respectively. We obtain

$$\mathbf{t}_E = \int \frac{-u_R}{r^2 - 1}d\lambda + C_E, \quad \mathbf{t}_L = \int \frac{u_I}{r^2 - 1}d\lambda + C_L,$$

where C_E and C_L are constants of integration. We will fix them by fixing a reference geodesic G_0 . We choose it as the geodesic with time separation $-i\frac{\beta}{2}$, which is the same as geodesic C in Fig. 3 (a). So knowing u_R and u_I is equivalent to knowing \mathbf{t}_E and \mathbf{t}_L . In other words, we assign $u = 0$ to the geodesic G_0 and use other u to measure how other geodesics are different from G_0 in proper time separation. For example, if $u_I = 0$, then the change of the proper time from that of G_0 is zero in the Lorentzian section. If u_R is equal to zero, then the change of the proper time from that of G_0 is zero in the Euclidean section, that is to say the Euclidean time separation will always be the constant $-i\frac{\beta}{2}$.

Now come back to the semi-classical approximation of $\tilde{\mathcal{G}}_\beta^+(u, k)$ in (26). By applying (27), we get

$$\tilde{\mathcal{G}}_\beta^+(u, k) \sim \exp(\nu(iu \cdot \mathbf{t}(u, k) - \mathbf{l}(u, k) + L\mathbf{d}(u, k))).$$

The position space boundary two-point Green function (20) is therefore,

$$\tilde{G}_{12}(t, t'; k) \sim \int_{-\infty}^{\infty} du [\exp(-iu(t' - t - i\frac{\beta}{2})\nu) \exp(\nu(iu \cdot \mathbf{t}(u, k) - l(u, k) + Ld(u, k)))] \quad (31)$$

Evaluating by steepest descent methods, the integration (31) will be dominated by its evaluation at saddle points, which are solutions of $\frac{2dZ_0(u, k)}{du} = i(\Delta t - i\frac{\beta}{2})$. By identity (30), the saddle point equation implies

$$\mathbf{t} = \Delta t - i\frac{\beta}{2}. \quad (32)$$

That is to say, saddle points as frequencies under the identification (25) will be identified as geodesics with proper time separation equals to $\Delta t - i\frac{\beta}{2}$. This agrees with the physical picture we have in mind. However, under the same identification, frequencies which are not saddles correspond to geodesics with time separation not necessarily $\Delta t - i\frac{\beta}{2}$. This means that those geodesics may not join the two points which appeared in the two-point function. The reason is that the relation (25) is obtained in the semi-classical limit when the wave-particle duality holds. We have no reason to expect it to be physically meaningful beyond this limit. Finally, by substituting (29) into (31) and applying (32), we have

$$\begin{aligned} \tilde{G}_{12}(t, t'; k) &\sim \int_{-\infty}^{\infty} du \exp(-iu(\Delta t - i\frac{\beta}{2})\nu) \exp(\nu(-l(\mathbf{t}, \mathbf{d}) + iut - ikd)) \\ &\sim \sum_{u_i} \exp(-m(l_i(\mathbf{t}_i, \mathbf{d}_i) + ikd_i)), \end{aligned}$$

where the last term is obtained as a summation with respect to saddle points, labelled by i , and identification between ν and m is assumed. The previous $f_i(k)$ which appeared in (21) is obtained as ikd_i . Hence we induce a geodesic approximation (21) from the assumption of the identification (25).

4.3 Saddle points and the geodesic approximation II

Since (25) is a complex relation, the correspondence we obtained in the last subsection is only a formal correspondence unless a proper analytic continuation process is provided. We have already seen that the Green function can be analytically extended by specifying its branch cuts. We will provide an analytic continuation for the geodesic approximation and hence make the formula (21) rigorous. There are two steps involved to define an analytic continuation for the functions \mathbf{t} , l , d . The first step is to analytically continue $r_c(u)$ to an analytic function on the complex u -plane, and the second step is to deform the contour of integration to the complex r -plane.

For the first step, r_c is a solution of (28), or equivalently, $r(u)^4 + (k^2 - u^2 - 1)r(u)^2 - k^2 = 0$. If the discriminant $(k^2 - u^2 - 1)^2 + 4k^2 = 0$, then u is in the set

$$\{u = \pm k \pm i\} \cup \{u = \pm k \mp i\}.$$

Observe that these points are located at the four end points of branch cuts of momentum space Green function at the large ν limit as in Fig. 2. In this case, $r(u)$ has a root of multiplicity 4. While the discriminant is not zero, there are four distinct roots. We will only concentrate on the one given as,

$$r_c(u) = +\sqrt{\frac{1}{2} \left(-k^2 + u^2 + 1 + \sqrt{(k^2 - u^2 - 1)^2 + 4k^2} \right)}. \quad (33)$$

It can be analytically continued to the complex u -plane if we cut the points where the discriminant is zero. Since properties we are concerned with do not differ much qualitatively when k varies as a positive real number, we will fix $k = 1$ from now on. We plot the real part and the imaginary part of the analytically continued function of (33) in Fig. 4.

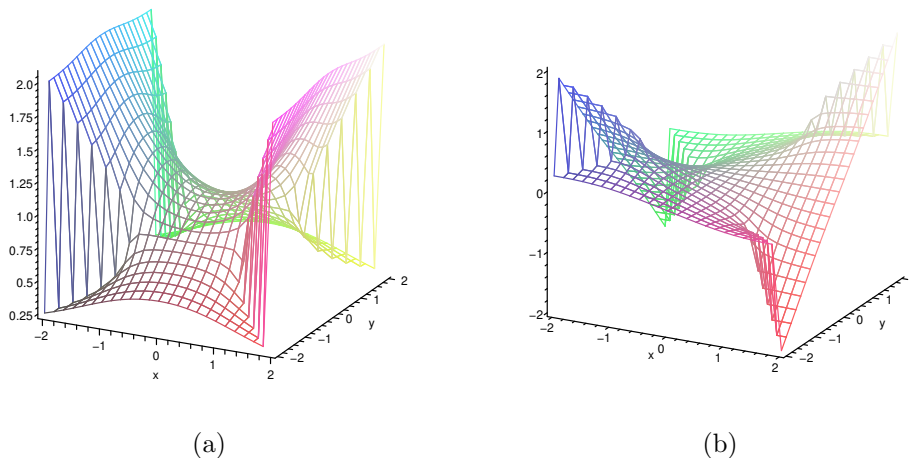


Figure 4: Fig. (a) is the real part of $r_c(u)$ on the complex $u = x + iy$ -plane when $k = 1$. Fig. (b) is the imaginary part of $r_c(u)$ on the complex u -plane when $k = 1$.

We want to mention some properties of the analytic function $r_c(u)$. When u approaches imaginary infinity, the norm of the turning point $|r_c(u)|$ approaches 0 and hence so does $r_c(u)$. As u approaches real infinity, the norm of the turning point approaches positive infinity. As u approaches 0 from any direction, the norm $|r_c|$ approaches one. $u = 0$ corresponds exactly to our reference geodesic G_0 . In particular, as u approaches 0 in the direction along either the real axis

or the imaginary axis, the imaginary part of $r_c(u)$ vanishes. Hence the analytic function $r_c(u)$ approaches the horizon at $r = 1$ in these two cases.

To understand the function $r_c(u)$ mathematically is quite simple. As the way we obtained, it is a holomorphic function coming from an analytic continuation of some function on the real line. Certain limiting behaviours mentioned above are quite neat. Meanwhile its physical explanation is not as clear as its mathematical explanation. The first problem which occurs is that the concept of turning point loses its usual physical meaning. For example, with a particular turning point of a complex value, we don't know how to compare it with the horizon at $r = 1$. Take its norm? Take its real part or anything else? So when we see this analytic function $r_c(u)$ we keep in mind that it is a nice function coming from a real function, which has physical meaning. If we want to use it, we use it in a way related to the original real function. Now consider the complex u -plane, the complex r -plane and the analytic function r_c which maps u to r . Physically, there are two distinct positions on the r -plane: the point $r = 1$ is the event horizon and the origin $r = 0$ is the singularity of the black hole. The previous observation concerning the function $r_c(u)$ tells us that it approaches $r = 1$ when u approaches zero along any direction. Therefore, we consider simply all straight lines, $u = |u| \exp(i\theta)$ with some constant θ , through the origin on the u -plane and find their images under $r_c(u)$ on the complex r -plane. Particular cases of this mapping are plotted in Fig. 5. Consider points on the line $u = |u| \exp(i\theta)$

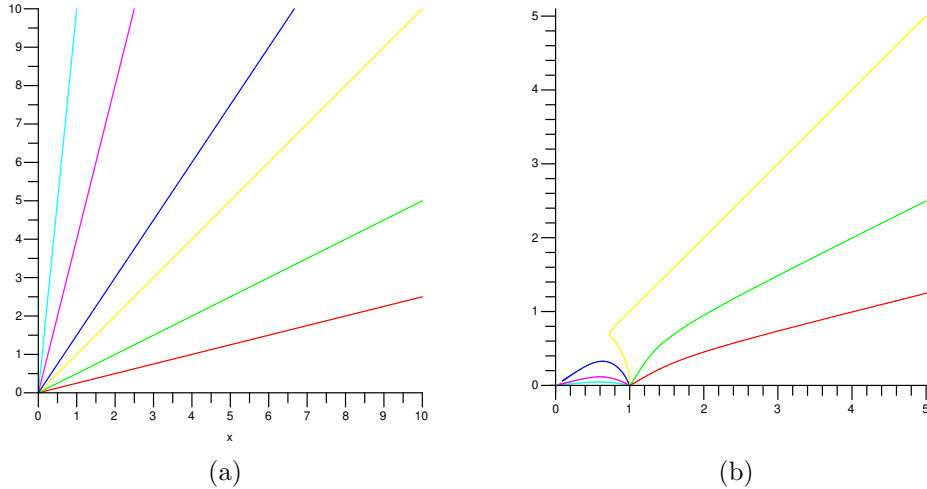


Figure 5: (a) shows straight lines $u = |u| \exp(i\theta)$ with varies slopes. (b) shows the images of $r_c(u)$ of the lines in (a). Lines and their images are of the same colour.

starting from zero to the complex infinity. The analytic function $r_c(u)$ thus gives us a family of geodesics parametrised by their turning point $r_c(u)$ as u moves.

No matter what θ is, the starting geodesic is the one with turning point at the horizon, which is G_0 . Therefore, we find a way to put any geodesic with an arbitrarily complex $r_c(u)$ into a family of geodesics by joining the origin to the u . This family is considered to consist of deformation of the reference geodesic G_0 . When $\theta = 0$, u is always real, and the family of geodesics are physically observable geodesics with real turning points starting from the horizon (G_0) to positive spatial infinity. When $\theta = \frac{\pi}{2}$, the line parametrises a family of geodesics with all real valued turning points, starting from horizon (G_0) and decrease monotonically to the spatial singularity at $r = 0$. Incidentally any line with θ greater than $\frac{\pi}{4}$ (this particular angle actually depend on our assumption of $k = 1$, other k will give other angle) has turning point $r_c(u) = 0$ as u goes to infinity. (Fig. 5)

As to the second step, the original contour in the integrations **t**, **l**, **d** as in (5), (6), (7) starts from $r_c(u)$ and goes to infinity along the real r -axis. As $r_c(u)$ is analytically continued into the complex r -plane, we need to specify the contour of integration. Although the deformation of the contour can be arbitrary, we would like to make a choice so that the heuristic relation (21) gives a proper geodesic approximation of the correlator. Since when $r_c(u)$ is very far from the horizon, the choice of contour is not easy to make, we will start by considering when $r_c(u)$ gets close to the horizon at $r = 1$. Write $r_c(u) = 1 + \epsilon \exp(i\eta)$ where ϵ is a sufficient small positive number and η ranges from 0 to 2π . Recall that $r_c(u)$ and $u = |u| \exp(i\theta)$ are in one-one correspondence as shown in Fig. 4 or Fig. 5. We will decide our contours according to the way how $r_c(u)$ approach to 1 with respect to η and hence to θ . As u approaches to 0^+ from $+\infty$ along the real axis ($\theta = 0$), they are proposed to relate to geodesics with difference in proper time from the geodesic G_0 only in the Euclidean section. Their turning points vary from $r = +\infty$ to $r = 1$. For example, geodesics A , B and C plotted in (b) of Fig. 3. This is actually the case before analytical continuation, so we simply choose the original contour as in (a) of Fig. 6. In this case, we can see that the pole at horizon does not contribute. This immediately implies the choice of the contour for u approaches to 0^- from $-\infty$ along the real axis ($\theta = \pi$) as in Fig. 6 (b). Indeed, simply consider a closed contour in (a) of Fig. 3: it starts at $\tau = 0$, $r = \infty$, and then goes very close to the horizon and finally goes to $r = \infty$ (as C). After this, it moves downwards along the arc a little bit and comes back along the dashed geodesic, which is very close to the horizon. Finally it goes back to the point where it starts. Integration along this closed contour will give proper time difference by $2\pi i$. While we have already chosen the contour as (a) of Fig. 6 so that the outwards geodesic avoids the singularity, we have to make a choice so that the backwards geodesic can pick up the factor of $2\pi i$. The contour in (b) of Fig. 6, when circling around the pole, picks up this factor. Hence the choice is confirmed.

That leaves us two more directions to consider. For the purpose of making a geodesic approximation, we are interested in geodesics joining two boundaries as

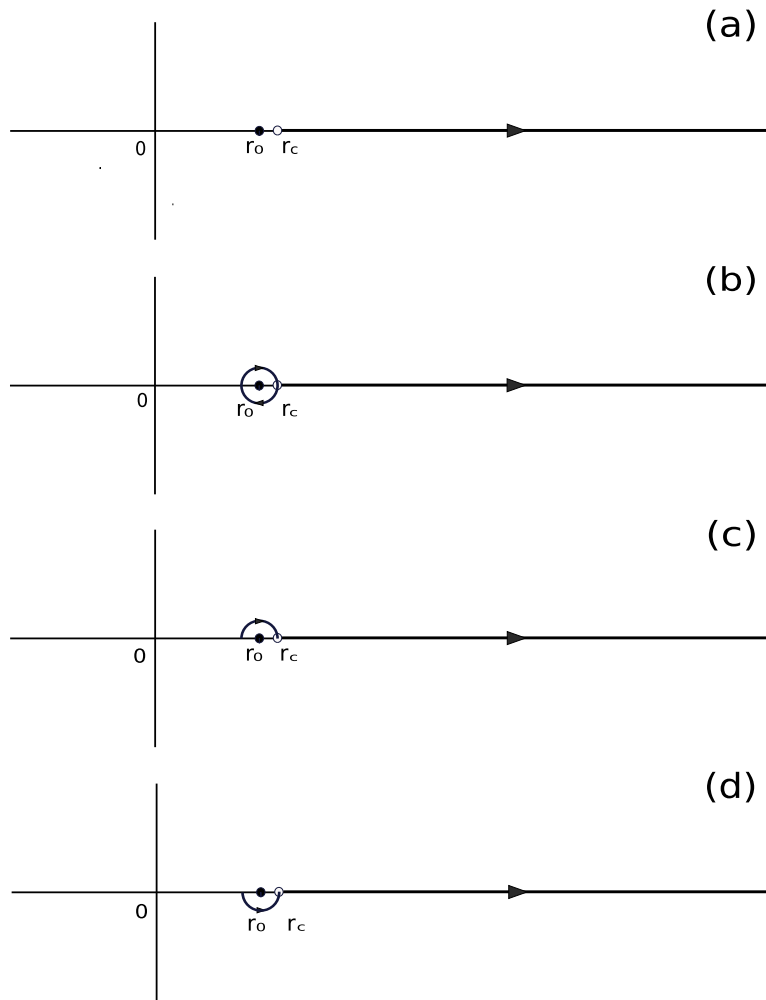


Figure 6: Choices of deformed contours. (a) The contour chosen for u approaches to 0^+ along the real axis. (b) The contour chosen for u approaches to 0^- along the real axis. (c) The contour chosen for u approaches to $i0^+$ along the imaginary axis. (d) The contour chosen for u approaches to $i0^-$ along the imaginary axis.

A , B , $C(G_0)$ and D in the Penrose diagram in Fig. 3. These geodesics correspond to $u = iu_I$, since there are no Euclidean time difference between them and the reference geodesic G_0 . The imaginary part u_I is indeed related to the Lorentzian proper time of the geodesics, since the Lorentzian time separation of G_0 is zero. We want to make a choice of contour so that the jumping in the Euclidean time $-i\frac{\beta}{2}$ is included even if we only carry out the integration for the Lorentzian section. As u_I moves from $+i\infty$ to 0 along the imaginary axis, $r_c(u_I)$ moves from $r = 0$ to the horizon along the real axis. As $r_c(u_I)$ goes very closed to $r = 1$, we choose the contour to be (c) of Fig. 6 so that this naturally include the jumping of $-i\frac{\beta}{2}$ by making use of the pole. Symmetrically, as u_I moves from $-i\infty$ to $i0^-$ along the imaginary axis, the contour is chosen as (d) of Fig. 6.

Therefore, for the turning point very closed to the horizon, we have made our choices for $\theta = 0, \frac{\pi}{2}, \pi, \frac{3\pi}{2}$ as in (a), (c), (b), (d) in Fig. 6, respectively. We make the following requirement for the rest of the θ 's: when $0 \leq \theta < \frac{\pi}{2}$, the contour is chosen to be as in (a); when $\frac{\pi}{2} \leq \theta < \pi$, the contour is chosen to be as in (c); when $\pi \leq \theta < \frac{3\pi}{2}$, the contour is chosen to be as in (b); when $\frac{3\pi}{2} \leq \theta < 2\pi$, the contour is chosen to be as in (d). As to u away from 0, i.e. $|u|$ not very small, $r_c(u)$ is far from the horizon. We simply choose the contour according to the argument θ of u .

Combining the two steps, we obtain a complete analytic continuation procedure. In this way the previous heuristic relation (21) is exactly defined. A interesting phenomenon is that the Lorentzian section of geodesics, which is related to the imaginary part of the saddle points, can have turning point inside horizon. In this sense, we may be able to find a signature of the BTZ singularity from the boundary correlation function. However, we by no means imply this is the only possible geodesic approximation. It is possible to assign different correspondence for u and r_c firstly, then to define a corresponding analytic continuation according to its relation with the correlation functions secondly. That is to say, it is possible to define a different way of geodesic approximation for the same correlation function. Similar ideas can be seen in [16], in which two different but equivalent analytic continuations for position space Green function are presented.

5 Application of the frequency-geodesic relation

With the exact geodesic approximation provided in the last section, we would like to see how it works through a simple computation and its physical implication. We will first look for saddle points of the correlation function (23) and then look for their corresponding geodesics. There are two cases of interest. The first case is when the time separation is purely Euclidean as in (b) of Fig. 3. The second case is when the two points sit on different boundaries in the Lorentzian section of space time with time separation $\Delta t - i\frac{\beta}{2}$ where Δt is the Lorentzian time

separation as in (a) of Fig. 3.

In the large ν limit, instead of finding $S_0(z)$ and hence $Z_0(u, k)$ as we did before, we adopt a slightly different procedure. Since we already have the explicit expression of the momentum space correlation function, we obtain the approximation simply by considering its asymptotic form in the large ν limit. After rescaling ω, J to u, k , we can write (20) in the form of (23) and get the expression of $2Z(u, k) = \frac{1}{\nu} \ln \tilde{\mathcal{G}}_\beta^+(u, k)$ as

$$\begin{aligned} 2Z(u, k) &= \frac{1}{\nu} [3\pi\nu u + \ln(\frac{\nu u}{2\pi\Gamma(1+\nu)^2}) \\ &\quad + \ln(\Gamma(\frac{\nu}{2}(iu + ik + 1 + \frac{1}{\nu}))) + \ln(\Gamma(\frac{\nu}{2}(iu - ik + 1 + \frac{1}{\nu}))) \\ &\quad + \ln(\Gamma(\frac{\nu}{2}(-iu + ik + 1 + \frac{1}{\nu}))) + \ln(\Gamma(\frac{\nu}{2}(-iu - ik + 1 + \frac{1}{\nu})))]. \end{aligned}$$

Applying the Stirling formula [30] to the Gamma functions appearing in $2Z(u, k)$, we get

$$\begin{aligned} 2Z(u, k) &= \frac{1}{\nu} [\ln(\frac{\nu}{2\pi\Gamma(1+\nu)^2}) + 2 \ln 2\pi - 2\nu - 2 + 2\nu \ln(\frac{\nu}{2})] \\ &\quad + \frac{1}{\nu} \ln(u) + 3\pi u + \frac{1}{2}(iu + ik + 1) \ln(iu + ik + 1) \\ &\quad + \frac{1}{2}(iu - ik + 1) \ln(iu - ik + 1) \\ &\quad + \frac{1}{2}(-iu + ik + 1) \ln(-iu + ik + 1) \\ &\quad + \frac{1}{2}(-iu - ik + 1) \ln(-iu - ik + 1). \end{aligned}$$

The derivative with respect to u and is then obtained as follows,

$$\frac{2dZ(u, k)}{du} = 3\pi + \frac{i}{2} \ln \frac{(iu + ik + 1)(iu - ik + 1)}{(-iu + ik + 1)(-iu - ik + 1)}, \quad \text{as } \nu \gg 1. \quad (34)$$

To carry out the steepest descent method, we may write (23) in the form of (22). In this way, $g(u)$ will be simply the constant ν and

$$h(u) = -iu \left(\Delta t - i\frac{\beta}{2} \right) + 2Z(u, k).$$

Saddles of $\tilde{G}_{12}(\Delta t - i\frac{\beta}{2}, k)$ are thus determined by $\frac{dh(u)}{du} = 0$, that is,

$$\frac{2dZ}{du} = i\Delta t + \frac{\beta}{2} \quad (35)$$

We write $\Delta t = t + i\tau$ for t and τ both real numbers, i.e. t is the time separation in Lorentzian section and τ is the time separation in the Euclidean section. We

can see that $t = 0$ is our first case where the time separation is purely imaginary. $\tau = 0$ corresponds to the second case. From (34) and (35), we can find saddle points by solving the following equation,

$$\frac{(iu + ik + 1)(iu - ik + 1)}{(-iu + ik + 1)(-iu - ik + 1)} = \exp(2(t + i\tau)),$$

where the inverse Hawking temperature $\beta = 2\pi$ is substituted in. There are two solutions,

$$u_{\pm}(\Delta t) = \frac{i(1 + \exp(2\Delta t)) \pm \sqrt{-4\exp(2\Delta t) + k^2(1 - \exp(2\Delta t))^2}}{1 - \exp(2\Delta t)}.$$

For simplicity, we will again assume $k = 1$. Computation can be carried out for other non-zero positive k similarly. When $t = 0$, we can view saddles as being parametrised by the Euclidean time τ . Since the Euclidean time separation τ is of period 2π , we may assume $\tau \in (-\pi, \pi]$. The saddles are

$$u_{\pm}^E(\tau) = \frac{i(1 + \exp(2i\tau)) \pm \sqrt{-4\exp(2i\tau) + (1 - \exp(2i\tau))^2}}{1 - \exp(2i\tau)}. \quad (36)$$

We observe that $u_{\pm}^E(\tau)$ have vanishing imaginary part. This implies that the time separation is purely Euclidean, the possible dominating geodesics of the correlation function will not have Lorentzian time section. Another observation from the solutions is that the two saddles are both periodic functions with respect to τ of period π . In particular, $u_{-}^E(\tau - \pi) = u_{+}^E(\tau)$. So there is in fact only one solution as seen in Fig. 7.

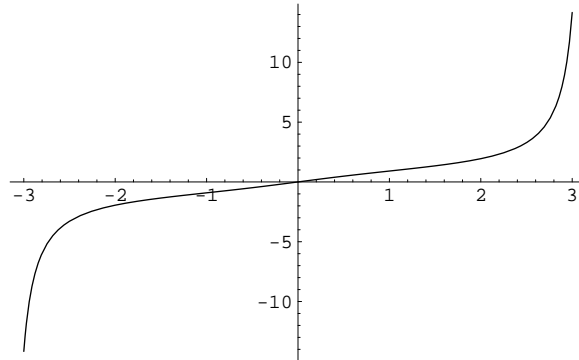


Figure 7: u_{\pm}^E parametrised by Euclidean time τ . As τ varies from $-\pi$ to 0, the graph of $u_{-}^E(\tau)$ is shown. As τ varies from 0 to π , the graph of $u_{+}^E(\tau)$ is shown.

Besides the formula (36), the behaviour of the saddle can be seen clearly from the graph of the correlation itself as in the left column of Fig. 8. As the Euclidean time difference τ increases from 0 to π , the saddles move from 0 to the right along

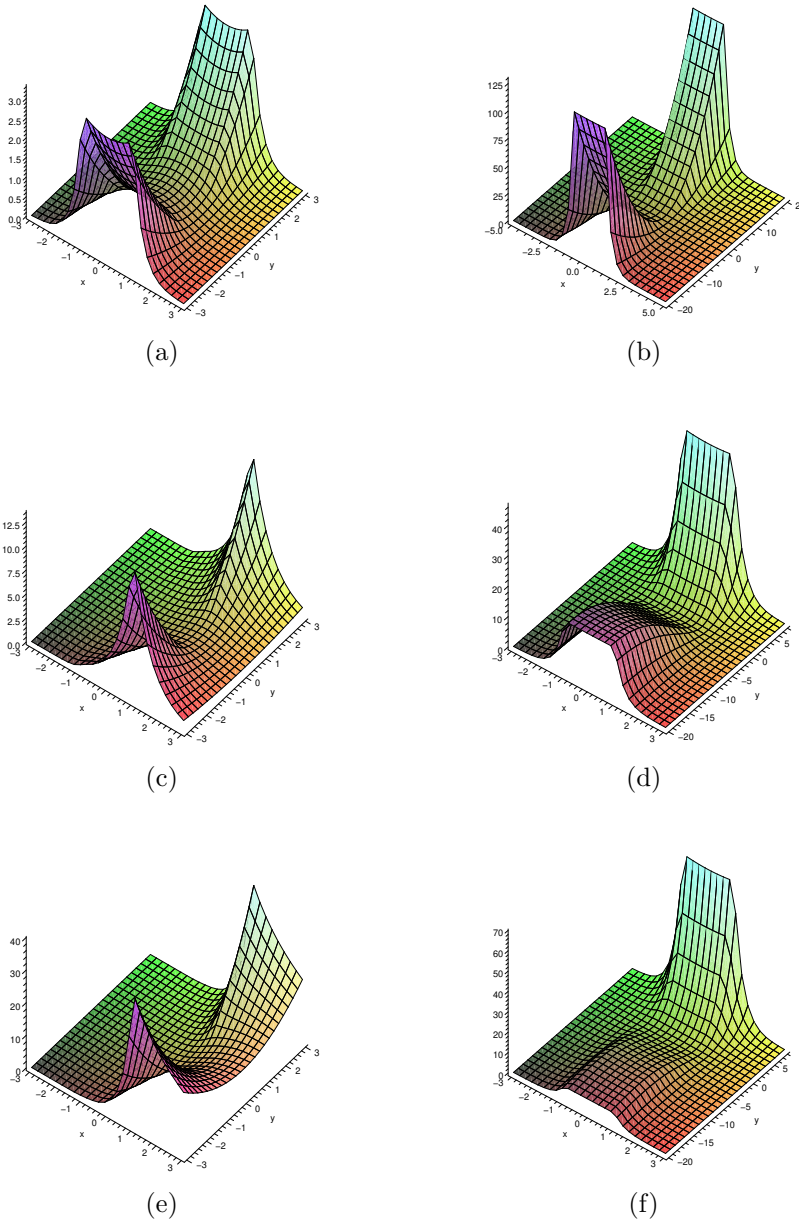


Figure 8: Graphs of $|\exp(h(u))|$ on the complex u -plane. (a), (c) and (e) are parametrised by the Euclidean time separation τ when $t = 0$. (a) is when $\tau = 0$, the saddle is at $u = (0, 0)$. (c) is when $\tau = 1.5$. (e) is when $\tau = 2.5$. (b), (d) and (f) are parametrised by the Lorentzian time separation t when $\tau = 0$. (b) is when $t = 0$. (d) is when $t = 0.1$, the upper saddle moves downwards and the lower one moves upwards rapidly. (f) is when $t = 1.5$, the two saddles stops at the lines $x = \pm 1$.

the real u -axis. For the limiting case when $\tau = \pi$, the saddles actually move to positive infinity. The changing of the shape of the graph is with respect to the moving of the saddle. Symmetrically, when τ varies from 0 to $-\pi$, the saddle starts from the origin and move to left till negative infinity along the real axis (not shown in the figure).

By evaluating the second derivative $\frac{d^2 h(u)}{du^2}$ at the saddles, we find that the saddle in this case is of degree one for all $\tau \in (-\pi, \pi]$ and the steepest descent contour is the real axis itself. Thus in this case, there is no need to deform the integration contour, and the saddle obtained dominates the integration.

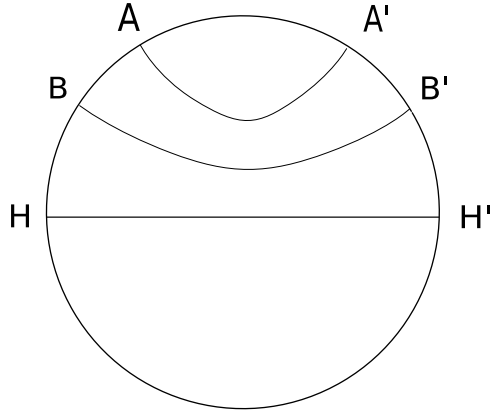


Figure 9: As saddle moves from the origin to the positive real axis, the corresponding geodesic moves from $H'H$ (i.e. G_0) to $B'B$ and then $A'A$.

According to the frequency-geodesic relation specified in the last section, we can find the corresponding geodesics with the saddle points. These geodesics will play the role of dominating geodesics in the geodesic approximation of the two-point function. As illustrated in Fig. 9, as u increases from 0, the corresponding geodesic moves from $H'H$, to $B'B$ and then $A'A$. As the saddle increase, the turning point of the corresponding geodesic move from the horizon to infinity. This is also what we expect.

The second case we want to consider is $\tau = 0$. Saddles are parametrised by the Lorentzian time t and given as

$$u_{\pm}^L(t) = \frac{i(1 + \exp(2t)) \pm \sqrt{-4 \exp(2t) + (1 - \exp(2t))^2}}{1 - \exp(2t)}. \quad (37)$$

Saddles are plotted as in the Figure 10. For each time t between 0 and ∞ there are two saddle points. As t varies from 0 to around 0.88, the upper saddle moves from the origin downwards to $-i$ and the lower saddle moves from negative imaginary infinity upwards to $-2i$ rapidly. The two saddles “meet” when the time separation is about 1.10. After that, the upper saddle moves to the left and the

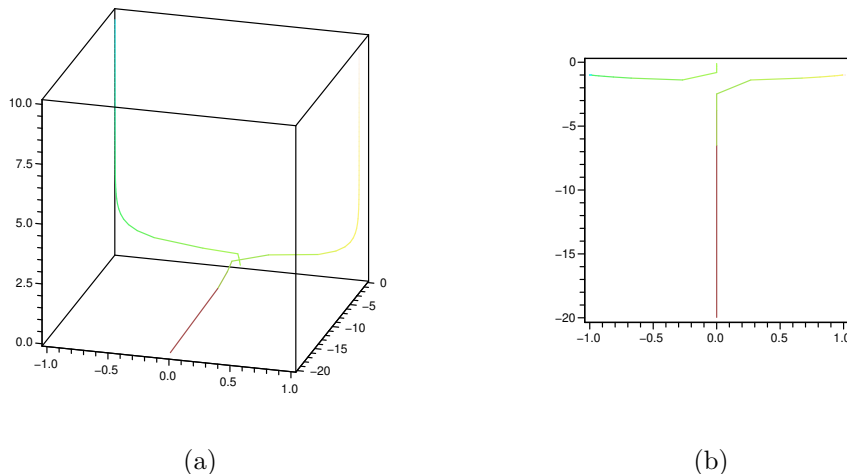


Figure 10: (a) Two trajectories of the upper and lower saddles $u_{\pm}^L(t)$ parametrised by Lorentzian time t (increases in the vertical direction) on the complex u -plane. (b) is the projection of (a) onto the complex u -plane.

lower one moves to the right, both with constant imaginary part. After the time separation exceeds $t = 1.7$, the two saddles disappear into the branch cuts around $u = \pm 1 - i$. A magnified picture indicating the “collision” of the upper and lower saddles is shown in Fig. 11.

The behaviour of saddles can also be seen from the graph of the correlation function itself as shown in the right column of Fig. 8. When the Lorentzian time separation is zero, the upper saddle is at the origin and the lower one is at $-i\infty$. There are two “lumps” (both diverge at infinity) in the graph. We refer them as the upper and lower part. As the time separation increase, the lower part descend (this corresponds to the lower saddle, who always sits on top the “lump”, moving upwards) and the upper parts at the same time grow. When the time separation becomes sufficiently large, the lower part almost becomes flat and the upper part grows very tall.

These are both of the saddles solved as solutions of $\frac{dh(u)}{du} = 0$. However, not all saddle points will contribute in the final approximation. We need to find out their steepest descent direction and decide which one can be used in the approximation. If we evaluate the second derivative $\frac{d^2h(u)}{du^2}$ at the saddles obtained, we can determine the steepest descent direction for each saddle. This is also indicated in Fig. 11. We can see that before the two saddles collide, the upper saddle has steepest descent direction in the horizontal direction. The lower saddle has its steepest descent in the vertical direction. Since the contour of the Fourier integration is along the real u -axis, we conclude that the dominant saddle is the upper one. In the cases when the saddles are colliding and after collision,

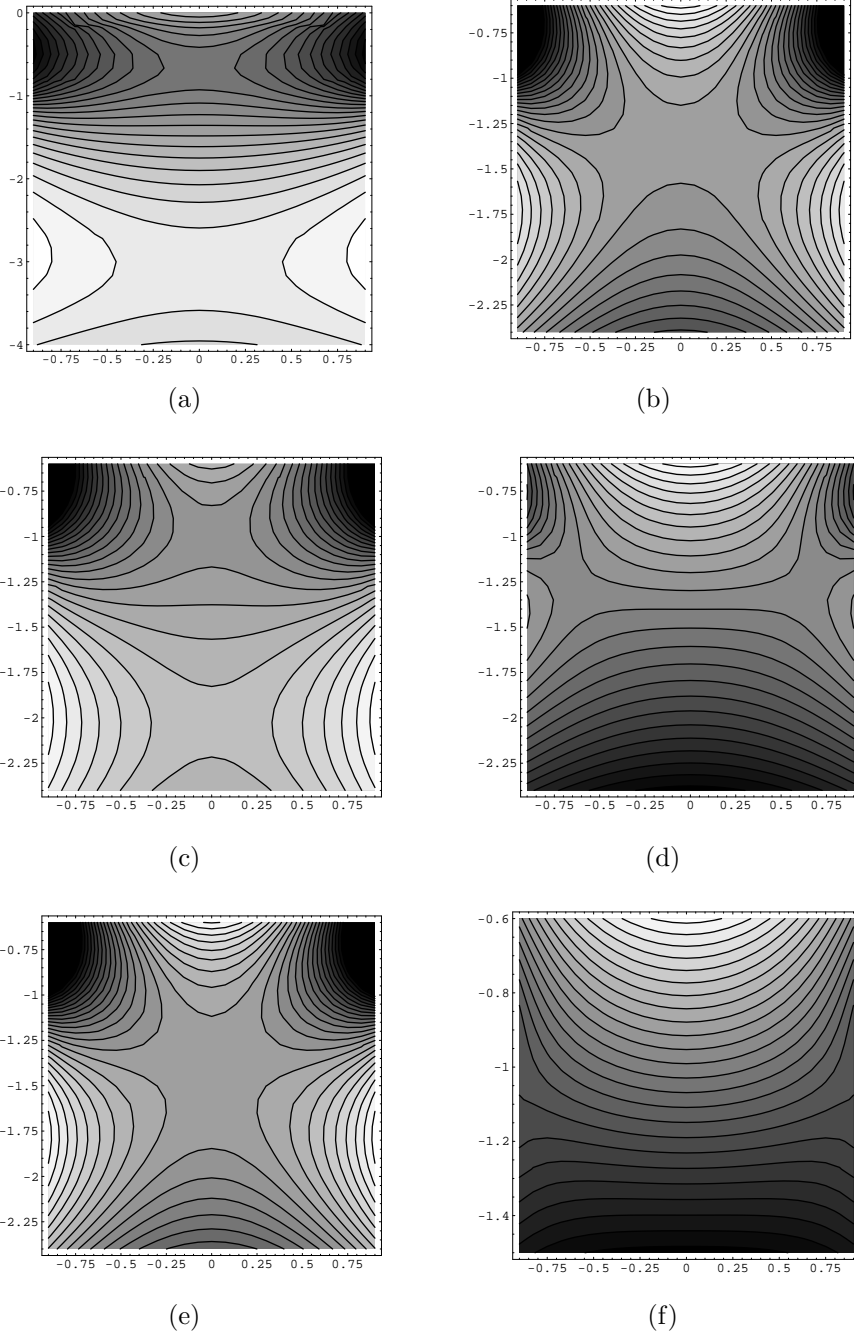


Figure 11: Saddles move with respect to Lorentzian time separation t . (Suggest to read the left column first and then the right one.) Shading in the figure has the property: darker means lower and lighter means higher. (a) $t = 0.60$. (c) $t = 0.80$. (e) $t = 0.88$. (b) $t = 0.90$. (d) $t = 1.10$. (f) $t = 1.70$. The upper saddle dominates in (a), (c) and (e). Both saddles dominate in (d). Saddles disappear on to the branch cut in (f).

their positions and steepest contours are symmetric with respect to the y axis, so both of the saddles contribute.

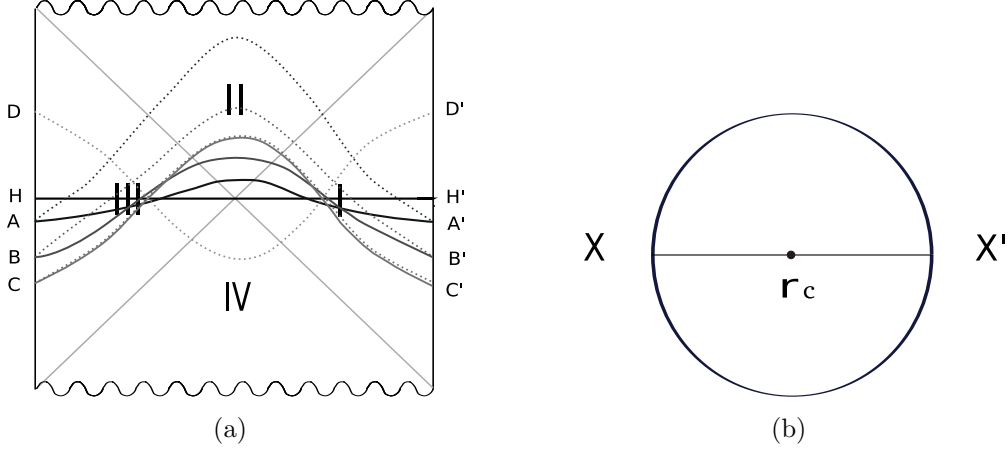


Figure 12: Geodesics in the Lorentzian and Euclidean sections before the saddle points collide. (a) The Lorentzian section. Geodesics with solid lines correspond to the upper dominating saddle at various time separation. Geodesics with dashed lines correspond to the lower not-dominating saddle at various time separation. (b) The Euclidean section at time separation t . When $t = 0$, $X'X = H'H$ and $r_c = 1$. As t increases, $X'X$ stands for $A'A$, $B'B$ and finally $C'C$, with r_c their corresponding turning points.

Now we would like to see how movements of saddle points imply the geodesic approximation. At $t = 0$, the upper saddle is at the origin $u = 0$, and this corresponds to the reference geodesic G_0 . This geodesic is shown as HH' in (a) of Fig. 12. The lower saddle is at imaginary infinity and does not count as a saddle yet. When the Lorentzian time separation t increases (from $H'H$, to $A'A$, $B'B$ and finally to $C'C$ in (a) of Fig. 12), the upper saddle moves downwards; the lower saddle moves upwards. Correspondingly, for solid geodesics (related to the upper saddle, which is dominant), their turning points move from the horizon to inside the horizon. For dashed geodesics (related to the lower saddle, which is not dominant), their turning points come out from the singularity but remain inside the horizon. When the Lorentzian time separation increases to $C'C$, which is related to the “collision” of the two saddles, the solid geodesic and the dashed one almost coincide. Consider projections of these geodesics onto the Euclidean section. Since the relating saddles both have vanishing real part, both projections will have time separation exactly $-i\frac{\beta}{2}$ as the reference geodesic G_0 . Therefore, for any geodesic appearing in (a), we can plot the centre of the circle to be its turning point r_c . Then the Euclidean projection of the geodesic will be $X'X$. $X'X$ stands for $H'H$, $A'A$, $B'B$ or $C'C$, and r_c depends on geodesics specified.

Before the collision of the saddles, the dominating geodesic is always the solid

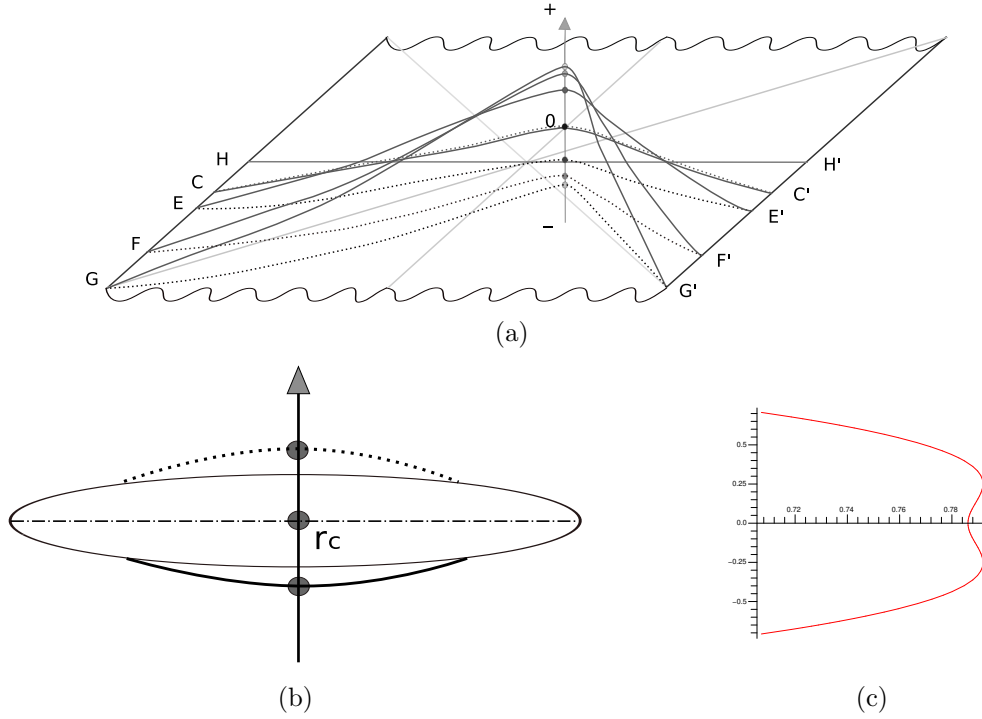


Figure 13: The spacetime related to the cases of collision and after collision of the two saddles. (a) The Lorentzian section. Solid eodesics correspond to the left saddle, which is from the previous upper one. Dashed geodesics correspond to the right saddle, which is from the previous lower one. (b) The Euclidean section. After the collision of saddles, there are two geodesics dominating simultaneously. The solid geodesic corresponds to the left saddle and the dashed geodesic corresponds to the right saddle. (c) After collision, the turning points pick up imaginary part of opposite sign. Real part of r_c is in the horizontal direction and imaginary part of r_c is in the vertical direction. As time increases, the two points start from the real axis, and split to upper and lower direction in a symmetrical way. This is the precise image of the vertical arrowed lines in (a) and (b).

one. After the saddles collide, the saddles pick up real part frequencies at the same time and both saddles make an equal contribution in the final approximation. (See Fig. 10). Correspondingly, there appear two dominating geodesics. They both have Euclidean time difference with respect to the reference geodesic G_0 . However, since their differences is of opposite sign, the summation of their Euclidean time difference with respect to G_0 remains 0. For both of the geodesics, their turning points are no longer real valued. So we need to extend both the Euclidean section and the Lorentzian section in a third dimension to indicate the direction of the imaginary part of the turning points r_c as shown in (a), (b) of Fig. 13. The magnified version of the third dimension is shown in (c) of Fig. 13. When the saddles collide, it is indicated as $C'C$ in (a) of Fig. 13. The two very close geodesics still lie inside the two-dimension Penrose diagram, with their real turning points inside the horizon. Let solid geodesics correspond to the left saddle, which is from the previously upper one and dashed geodesics correspond to the right saddle, which is from the previously lower one. As time separation increases from $C'C$, to $E'E$, $F'F$ and then to $G'G$, turning points of the solid geodesic now slowly rise above the Penrose diagram. Their turning points have almost constant real part and increasing imaginary part. This is shown as the upper half of (c) in Fig. 13. At the same time, the turning points of the dashed geodesic now slowly descends to underneath the Penrose diagram. They are again with almost constant real part, but decreasing imaginary part. It is shown as the lower half of (c) in Fig. 13.

The Euclidean sections of these geodesics are less simple to describe. For the pair of dominating geodesics, (except for $C'C$,) in (a) of Fig. 13, there are two corresponding geodesics in the Euclidean section as their projections. The two images have opposite time differences with respect to $-i\frac{\beta}{2}$ and with same real parts and opposite imaginary parts of turning points. They are indicated in (b) of Fig. 13. The solid geodesic is the projection of the solid geodesics from (a) and the dashed geodesic is the projection of dashed one from (a). The centre of the disk is decided by the real part of the turning points of various geodesics.

In summary, for the time separation being Euclidean as $i\tau - i\frac{\beta}{2}$, one saddle point appears. This implies that for the geodesic approximation, there is one dominant geodesic for each τ . This geodesic has purely Euclidean proper time $i\tau - i\frac{\beta}{2}$. As τ increase, the turning point of the geodesics varies from the horizon to the infinity. For the time separation being $t - i\frac{\beta}{2}$, there are always two saddle points appearing as solutions of the saddle point equation. However, they don't both dominate all the time. As t increases from 0 to the time when the two saddles collide, only the upper saddle dominates. The corresponding geodesic approximation tells us that the dominating geodesic starts from the one with time separation $-i\frac{\beta}{2}$ and turning point at the event horizon, i.e. G_0 . As t increases, the turning point of the geodesic moves inside to the horizon. At the same time, the turning point of the other (not dominant) geodesic is moving

from deep inside the singularity outwards. We will make more comment in the next paragraph on the non-dominating partner. By the time the saddles collide, the two geodesics almost coincide. After that, two geodesics contribute equally in the geodesic approximation. They always have the same real part of turning point and opposite sign imaginary parts of the turning point. As t increases, real parts of their turning points stay inside the horizon not changing much, around 0.7 to 0.8 (see (c) of Fig. 13), while imaginary parts increase in same amount in norm. In the Euclidean section, the two dominating geodesics have time difference $-i\frac{\beta}{2} + i\delta$ and $-i\frac{\beta}{2} - i\delta$, rather than before when there is only one dominating geodesic with time separation $-i\frac{\beta}{2}$. We have seen that some of the dominating geodesics depending on the time separation have turning points inside the horizon. In this sense, we say that the boundary correlation function encodes locations inside the event horizon. On the other hand, in all the cases, the turning points never go infinitely closed to the singularity. This surely is not good enough for the purpose of resolving singularity.

As we mentioned, when the time difference is $t - i\frac{\beta}{2}$ for t quite small, there appears the lower saddle. It moves from $-i\infty$ upwards along the imaginary axis. Its steepest descent direction is always along the imaginary axis. Recall that at the same time the upper saddle always has steepest descent direction in the horizontal direction. This implies that when the steepest descent method is applied, the lower one is not picked up because of the contour of integration is along the real axis. We can define a function from the original Fourier integration by replacing the contour of integration by the imaginary axis as an analogue of the new observable proposed in [20] for AdS_5 black hole. Despite the fact that the new integration actually blows up and assuming a regularization is available, we study it as a regularized mathematical function. If we apply the steepest descent method as before, the lower saddle rather than the upper one will become dominant. That is to say, if this new function has any physical meaning to anybody, wavepackets can move along the geodesic with turning point deep inside the horizon at the semi-classical limit. The smaller the time separation t is, the deeper the particle can go. As t approaches zero, the turning point approaches infinitely close to the singularity. In this way, the newly defined function as a function on the boundary carries information from the singularity and may help in resolving the BTZ black hole singularity. At the same time, we should admit that its physical meaning is not clear.

6 Conclusion

The main objective of this paper is to see how the two-point function in the boundary CFT carries signatures from inside the horizon of the BTZ black hole in the context of the AdS/CFT correspondence. By using the key identification

between frequencies and geodesics in the semi-classical limit in [20], we deduce a geodesic approximation from the saddle point approximation. As an application, we compute the Hartle-Hawking Green function by mode summation directly and obtain the boundary two-point function by the AdS/CFT correspondence. By taking the semi-classical limit, we find saddle points of the two-point function with respect to the time separation and thus relate the saddle points to specific dominating geodesics on the bulk. There are two interesting features which appear. The first occurs when the time separation is $t - i\frac{\beta}{2}$, for the Lorentzian time separation t not very small. There are two dominant geodesics with turning points complex conjugate of each other and also with Euclidean time separations $-i\frac{\beta}{2} + i\delta$ and $-i\frac{\beta}{2} - i\delta$, respectively. This indicates the approximation of the two-point function is given by two complex geodesics together. The second interesting feature appears when the time separation is $t - i\frac{\beta}{2}$ for the Lorentzian time separation t not very far from zero. If we replace the original integration contour in the Fourier integration of the position space two-point function by the imaginary axis and regularize the new integration, then the saddle picked up with respect to the new contour is the one who can have turning point infinitely closed to the singularity. If there is good explanation about the newly defined function in the boundary theory, it may help to resolve the singularity.

Appendix

We will fix constants C_1 and C_2 so that the boundary conditions (14) are satisfied. We will get an approximate form of the solution around boundary first and fix the constraint between C_1 and C_2 by imposing the boundary condition (14). As $r \rightarrow \infty$, $z \sim \frac{1}{r} \rightarrow 0$, the approximated solution is

$$X_{bdry}(z) = (-1)^{-\frac{i\omega}{2}} z^{-\frac{1}{2}} z^{i\omega} (C_1 z^{iJ} G(z) + C_2 z^{-iJ} H(z)),$$

where

$$G(z) = F\left(\frac{-iJ - i\omega + 1 - \nu}{2}, \frac{-iJ - i\omega + 1 + \nu}{2}; 1 - iJ, \frac{1}{z^2}\right),$$

$$H(z) = F\left(\frac{iJ - i\omega + 1 - \nu}{2}, \frac{iJ - i\omega + 1 + \nu}{2}; 1 + iJ, \frac{1}{z^2}\right).$$

From general identities of hypergeometric function [30], we can further approximate the solution by

$$X_{bdry}(z) = (-1)^{-\frac{1}{2}} ((C_1 (-1)^{-\frac{-iJ-\nu}{2}} \Gamma_1 + C_2 (-1)^{-\frac{iJ-\nu}{2}} \Gamma_2) z^{\frac{1}{2}-\nu} \quad (38)$$

$$+ (C_1 (-1)^{-\frac{-iJ+\nu}{2}} \Gamma_3 + C_2 (-1)^{-\frac{iJ+\nu}{2}} \Gamma_4) z^{\frac{1}{2}+\nu}), \quad (39)$$

where

$$\Gamma_1 = \frac{\Gamma(1 - iJ)\Gamma(\nu)}{\Gamma(\frac{1}{2}(1 - i\omega - iJ + \nu))\Gamma(\frac{1}{2}(1 + i\omega - iJ + \nu))},$$

$$\begin{aligned}\Gamma_2 &= \frac{\Gamma(1+iJ)\Gamma(\nu)}{\Gamma(\frac{1}{2}(1-i\omega+iJ+\nu))\Gamma(\frac{1}{2}(1+i\omega+iJ+\nu))}, \\ \Gamma_3 &= \frac{\Gamma(1-iJ)\Gamma(-\nu)}{\Gamma(\frac{1}{2}(1-i\omega-iJ-\nu))\Gamma(\frac{1}{2}(1+i\omega-iJ-\nu))}, \\ \Gamma_4 &= \frac{\Gamma(1+iJ)\Gamma(-\nu)}{\Gamma(\frac{1}{2}(1-i\omega+iJ-\nu))\Gamma(\frac{1}{2}(1+i\omega+iJ-\nu))}.\end{aligned}$$

Imposing the boundary condition by requiring $z^{\frac{1}{2}-\nu}$ mode of (38) vanish, we get the constraint between the constant C_1 and C_2 as

$$C_2 = -(-1)^{iJ} \frac{\Gamma_1}{\Gamma_2} C_1. \quad (40)$$

Thus, (38) becomes

$$X_{bdry}(z) = C(\omega, J) z^{\frac{1}{2}+\nu}, \quad (41)$$

where

$$\begin{aligned}C(\omega, J) &:= C_1 (-1)^{\frac{iJ-\nu-1}{2}} (\Gamma_3 - \frac{\Gamma_1}{\Gamma_2} \Gamma_4) \\ &= C_1 (-1)^{\frac{iJ-\nu}{2}} \frac{1}{\pi^2} \sin(\pi\nu) \sinh(\pi J) \\ &\quad \Gamma(-\nu) \Gamma\left(\frac{1-i\omega+iJ+\nu}{2}\right) \Gamma(1-iJ) \Gamma\left(\frac{1+i\omega+iJ+\nu}{2}\right).\end{aligned}$$

Next, we want to get the approximation of (13) around the horizon and impose boundary conditions to fix constants C_1 and C_2 completely.

Again by general properties of hypergeometric functions, the approximation of (13) around the horizon is

$$X_{hor}(r) = r^{\frac{1}{2}} ((C_1 \Gamma_5 + C_2 \Gamma_6) (1-r^2)^{-\frac{i\omega}{2}} + (C_1 \Gamma_7 + C_2 \Gamma_8) (1-r^2)^{\frac{i\omega}{2}}),$$

where

$$\begin{aligned}\Gamma_5 &= \frac{\Gamma(1-iJ)\Gamma(i\omega)}{\Gamma(\frac{1}{2}(1+i\omega-iJ+\nu))\Gamma(\frac{1}{2}(1+i\omega-iJ-\nu))}, \\ \Gamma_6 &= \frac{\Gamma(1+iJ)\Gamma(i\omega)}{\Gamma(\frac{1}{2}(1+i\omega+iJ+\nu))\Gamma(\frac{1}{2}(1+i\omega+iJ-\nu))}, \\ \Gamma_7 &= \frac{\Gamma(1-iJ)\Gamma(-i\omega)}{\Gamma(\frac{1}{2}(1-i\omega-iJ-\nu))\Gamma(\frac{1}{2}(1-i\omega-iJ+\nu))}, \\ \Gamma_8 &= \frac{\Gamma(1+iJ)\Gamma(-i\omega)}{\Gamma(\frac{1}{2}(1-i\omega+iJ-\nu))\Gamma(\frac{1}{2}(1-i\omega+iJ+\nu))}.\end{aligned}$$

In the z coordinates,

$$X_{hor}(z) = \exp\left(-\frac{\pi\omega}{2}\right)[(C_1\Gamma_5 + C_2\Gamma_6)2^{-i\omega} \exp(-i\omega z) + (C_1\Gamma_7 + C_2\Gamma_8) \exp(\pi\omega)2^{i\omega} \exp(i\omega z)].$$

By the constraint (40) from boundary,

$$\begin{aligned} X_{hor}(z) &= \exp\left(-\frac{\pi\omega}{2}\right)[(C_1\Gamma_5 - (-1)^{iJ}\frac{\Gamma_1}{\Gamma_2}C_1\Gamma_6)2^{-i\omega} \exp(-i\omega z) \\ &\quad + (C_1\Gamma_7 - (-1)^{iJ}\frac{\Gamma_1}{\Gamma_2}C_1\Gamma_8) \exp(\pi\omega)2^{i\omega} \exp(i\omega z)] \\ &= C_1 \exp\left(-\frac{\pi\omega}{2}\right)(2^{-i\omega}P \exp(-i\omega z) + 2^{i\omega}Q \exp(i\omega z)), \end{aligned}$$

where

$$P = \frac{(\exp(J\pi) - \exp(-J\pi))\Gamma(1 - iJ)\Gamma(i\omega)}{(\exp(J\pi) + \exp(\pi(\omega + i\nu)))\Gamma(\frac{1}{2}(1 + i\omega - iJ - \nu))\Gamma(\frac{1}{2}(1 + i\omega - iJ + \nu))},$$

$$Q = \frac{\exp(-\pi\omega)(\exp(J\pi) - \exp(-J\pi))\Gamma(1 - iJ)\Gamma(-i\omega)}{(\exp(J\pi) + \exp(\pi(-\omega + i\nu)))\Gamma(\frac{1}{2}(1 - i\omega - iJ - \nu))\Gamma(\frac{1}{2}(1 - i\omega - iJ + \nu))}.$$

Numerically, it turns out that $|P| = |Q|$. The boundary condition at the horizon implies that C_1 should be chosen as $C_1 = \exp(\frac{\pi\omega}{2})(PQ)^{-\frac{1}{2}}$. Indeed,

$$\begin{aligned} X_{hor}(z) &= \frac{\exp(\frac{\pi\omega}{2})}{\sqrt{PQ}} \exp\left(-\frac{\pi\omega}{2}\right)(2^{-i\omega}P \exp(-i\omega z) + 2^{i\omega}Q \exp(i\omega z)) \\ &= 2^{-i\omega} \sqrt{\frac{P}{Q}} \exp(-i\omega z) + 2^{i\omega} \sqrt{\frac{Q}{P}} \exp(i\omega z). \end{aligned}$$

If we define θ by $\exp(i\theta) = \sqrt{\frac{Q}{P}}$, then $|P| = |Q|$ implies that θ is real. Let $\delta = \omega \ln 2 + \theta$, then the solution is $X_{hor}(z) = \exp(i\omega z) \exp(i\delta) + \exp(-i\omega z) \exp(-i\delta)$, and hence satisfies the boundary condition. After C_1 is fixed, $C(\omega, J)$ is fixed and its square is given as,

$$\begin{aligned} C(\omega, J)^2 &= \frac{1}{2\pi^3} \exp(\pi\omega)(\exp(2\pi\omega) - 1)\omega \sin^2(\pi\nu)\Gamma(-\nu)^2 \\ &\quad \Gamma\left(\frac{1}{2}(i\omega + iJ + \nu + 1)\right)\Gamma\left(\frac{1}{2}(-i\omega + iJ + \nu + 1)\right) \\ &\quad \Gamma\left(\frac{1}{2}(i\omega - iJ + \nu + 1)\right)\Gamma\left(\frac{1}{2}(-i\omega - iJ + \nu + 1)\right). \end{aligned}$$

Acknowledgement

I want to thank my supervisor Mukund Rangamani for constant help through the process of writing this paper. I indebted him for firstly showing me the main paper [20], on which this work is based, secondly providing the method and computation of the momentum space correlation function by modes sum, where the constant $C(\omega, J)$ is crucial for the later analysis on saddle points, and thirdly for useful discussions and comments in the layout this paper. I also want to thank Derek Harland for lots of stimulating discussions and reading the manuscript.

References

- [1] Juan M. Maldacena. The large n limit of superconformal field theories and supergravity. *International Journal of Theoretical Physics*, 38:1113, 1999.
- [2] S. S. Gubser, I. R. Klebanov, and A. M. Polyakov. Gauge theory correlators from non-critical string theory. *Physics Letters B*, 428:105, 1998.
- [3] Edward Witten. Anti de sitter space and holography. *Advances in Theoretical and Mathematical Physics*, 2:253, 1998.
- [4] Vijay Balasubramanian, Per Kraus, and Albion Lawrence. Bulk vs. boundary dynamics in anti-de sitter spacetime. *Physical Review D*, 59:046003, 1999.
- [5] Vijay Balasubramanian, Per Kraus, Albion Lawrence, and Sandip Trivedi. Holographic probes of anti-de sitter spacetimes. *Physical Review D*, 59:104021, 1999.
- [6] Tom Banks, Michael R. Douglas, Gary T. Horowitz, and Emil Martinec. Ads dynamics from conformal field theory, 1998.
- [7] Igor R. Klebanov and Edward Witten. Ads/cft correspondence and symmetry breaking. *Nuclear Physics B*, 556:89, 1999.
- [8] Esko Keski-Vakkuri. Bulk and boundary dynamics in btz black holes. *Physical Review D*, 59:104001, 1999.
- [9] Ulf H. Danielsson, Esko Keski-Vakkuri, and Martin Kruczenski. Spherically collapsing matter in ads, holography, and shellons. *Nuclear Physics B*, 563:279, 1999.
- [10] Gary T. Horowitz and Simon F. Ross. Possible resolution of black hole singularities from large n gauge theory. *JHEP*, 9804:015, 1998.

- [11] Juan Maldacena and Andrew Strominger. Ads3 black holes and a stringy exclusion principle. *JHEP*, 9812:005, 1998.
- [12] Vijay Balasubramanian and Simon F. Ross. Holographic particle detection. *Physical Review D*, 61:044007, 2000.
- [13] Jorma Louko, Donald Marolf, and Simon F. Ross. On geodesic propagators and black hole holography. *Physical Review D*, 62:044041, 2000.
- [14] Samuli Hemming, Esko Keski-Vakkuri, and Per Kraus. Strings in the extended btz spacetime. *JHEP*, 0210:006, 2002.
- [15] Juan M. Maldacena. Eternal black holes in ads. *JHEP*, 0304:021, 2003.
- [16] Per Kraus, Hiroshi Ooguri, and Stephen Shenker. Inside the horizon with ads/cft. *Physical Review D*, 67:124022, 2003.
- [17] Lukasz Fidkowski, Veronika Hubeny, Matthew Kleban, and Stephen Shenker. The black hole singularity in ads/cft. *JHEP*, 0402:014, 2004.
- [18] Jared Kaplan. Extracting data from behind horizons with the ads/cft correspondence, 2004.
- [19] Alex Hamilton, Daniel Kabat, Gilad Lifschytz, and David A. Lowe. Local bulk operators in ads/cft: a boundary view of horizons and locality. *Physical Review D*, 73:086003, 2006.
- [20] Guido Festuccia and Hong Liu. Excursions beyond the horizon: Black hole singularities in yang-mills theories (i). *JHEP*, 0604:044, 2006.
- [21] A. Erdélyi. *Asymptotic expansions*. Dover Publications, Inc., 1956.
- [22] S. A. Fulling. Alternative vacuum states in static space-times with horizons. *J. Phys. A: Math. Gen.*, 10:917, 1977.
- [23] J. B. Hartle and S. W. Hawking. Path-integral derivation of black-hole radiance. *Physical Review D*, 13:2188, 1976.
- [24] Samuli Hemming and Esko Keski-Vakkuri. Hawking radiation from ads black holes. *Physical Review D*, 64:044006, 2001.
- [25] Samuli Hemming. *Aspects of Quantum Fields and Strings on AdS Black Holes*. PhD thesis, University of Helsinki, Helsinki, Finland, May 2004.
- [26] G. W. Gibbons and M. J. Perry. Black holes and thermal green functions. *Proc. R. So. Lond. A.*, 358:467, 1978.

- [27] Maximo Banados, Marc Henneaux, Claudio Teitelboim, and Jorge Zanelli. Geometry of the 2+1 black hole. *Physical Review D*, 48:1506, 1993.
- [28] N. D. Birrell and P. C. W. Davies. *Quantum fields in curved space*. Cambridge University Press, 1999.
- [29] N. Bleistein and R. A. Handelsman. *Asymptotic expansions of integrals*. Holt, Rinehart and Winston, 1975.
- [30] Milton Abramowitz and Irene A. Stegun, editors. *Handbook of mathematical functions*. Dover Publications, Inc., New York, 1972.